Enabling the direct comparison of high-resolution precipitation observations with operational weather prediction model output

Master Thesis in Meteorology

Mari Berntsen Steinslid

Supervisor: Harald Sodemann
Co-Supervisor: Marvin Kähnert

June 1, 2022

UNIVERSITY OF BERGEN
Faculty of Mathematics and Natural Sciences
Geophysical Institute

Abstract

Precipitation characteristics is expected to change in the future, as an effect of global climate change. High-intensity precipitation will become a more frequent concern in some areas of the world. The rapid changes and small scales of these precipitation events still pose a big challenge for the numerical weather prediction (NWP) models. High-resolution comparison of observations and model output could provide us with a more detailed understanding of the precipitation event and how it unfold in the model. In this thesis, I have worked on providing a methodology for directly enabling the comparison of observed high-resolution precipitation with operational weather prediction model output. A detailed dataset was extracted from the operational weather prediction model in Norway at every time step, for a user defined subdomain centered around the observation location. The high-resolution comparison proved to give detailed information about intensity and timing of the precipitation, which in comparison was smoothed out in hourly data. In addition, the model showed a lot of spatial variability. Location proved to be an important factor for which features of the observations was present and which was not. Overall the model performed well during the calmer periods of precipitation, while the high-intensity precipitation proved to be a challenge.

Acknowledgements

First of all, I want to thank my supervisor Harald Sodemann for guiding me through the whole process that comes with writing a MSc. In addition, I want to say how grateful I am for being included into the group and especially for being allowed to take part in the field experience with ISLAS2022.

Then, to my co-supervisor Marvin Kähnert, thank you for helping me through the work of learning a brand new tool and for always being patient with my many, many questions in regards to programming.

A huge thank you to my friends at GFI. I am so happy we were able to work together for all these years.

And, last but not least, thank you to my familiy for always supporting me, and for patiently listening to all my excited ramblings about this MSc.

Contents

1 Introduction

The weather is expected to intensify in the future. Precipitation is one of the parameters anticipated to have a significant change in behaviour. Particularly in regards to intensity, duration and frequency of events. High-intensity precipitation is defined by large amounts of water falling within a short period of time. The high intensity generates a risk of landslides, flooding and other hydrological hazards (Azad and Sorteberg, 2017), consequently leading to a risk for human lives and a potential for great material damage. The damage can be limited by sufficient warning and thus, time to prepare. Accurate forecasts become a necessity. Still, precipitation continues to be one of the main uncertainties in numerical weather prediction (NWP) models, making it a key focus of research.

A cycle of complex microphysical processes is the basis for precipitation formation (Läderach and Sodemann, 2016). The starting point is ocean evaporation, followed by transport and lifting, leading to saturation and condensation. Droplets are formed, other microphysical processes such as aggregation, accretion, autoconversion and the Wegener-Bergeron-Findeisen process ensures droplet growth (Rogers and Yau, 1989). The challenge with these processes are the rapid changes and very small scales, which the NWP model struggles to resolve. Parametrization of these processes becomes necessary. As a consequence, the microphysics in the model are simplified, and errors and uncertainties arise.

One of the main uncertainties for precipitation in NWP models, is the prediction of convective cells. In many regions of the world, these are the features most prone to cause severe intense precipitation periods, with potential for large damage. High-intensity showers during summer in Norway, for example, is often a result of such convective cells. They occur on a small local scale, with rapidly changing conditions, and require a high resolution in space and time.

Precipitation has usually been investigated on a time-resolution of 1 hour accumulated data or more. The operational weather prediction model in Norway, AROME-MetCoOp[1] for example, uses a default time-resolution of 1 hour for precipitation output (Müller et al., 2017). The forecasts communicated to the population is usually presented in hourly rain rate. In a characterization of stratoform precipitation moving over a coastal area, 3-hour resolution data was used (Zagrodnik et al., 2018). While Azad and Sorteberg (2017) worked with daily accumulated precipitation when linking extreme precipitation in the coastal areas of Norway to atmospheric rivers.

All of these examples provide valuable knowledge about the evolution of accumulated precipitation for different purposes. However, for some situations, a more detailed description of the precipitation development within this accumulated time period could be beneficial. We know that rapid changes in time provides a challenge for the models, as with the high-intensity showers. For this, a more detailed description of intensity, timing and intermittence could provide a better understanding of the precipitation event and how it unfolds in the model.

Observational data are available for a much higher time resolutions than hourly. This

[1]The Meteorological Cooperation on Operational Numerical Weather Prediction (MetCoOp) is a further development of the french model: Météo-France Applications of Research to Operations at Mesoscale (AROME).

provides a unique opportunity for obtaining detailed knowledge about the precipitation.

There are however fewer studies working with higher time-resolution. One example is the Norwegian Meteorological Institute's new live precipitation forecast (also called "nowcast"), users receive a detailed prediction of precipitation for the coming 90 minutes. The nowcast is based on radar data and updates every 5 minutes to give a more accurate representation of the current precipitation situation. In addition, this forecast uses a finer horizontal resolution of 1 km, compared to the usual 2.5 km for AROME-MetCoOp. The advantage of this combination of higher time and spatial resolution becomes clear from the fact that the nowcast manage to capture some of the local convective showers missed by the general model prediction (YR, 2022). This is not based on a NWP model, but it provides an example for how studies on higher time-resolution could be beneficial.

This brings forth another important aspect of the challenges in numerical weather prediction, namely spatial resolution. High-intensity precipitation often occur in complex topography areas. Mountains for example play a large role in enhancing the precipitation (Azad and Sorteberg, 2017). Still, the prediction in these areas is often uncertain, due to the fact that the model is unable to represent the true detail of the topography. Spatial resolution is the focus of numerous other studies e.g. Valkonen et al. (2020) who investigates the possible benefits of using a 0.5 km horizontal grid spacing in the complex Arctic terrain, and will not specifically be addressed here.

Another example of higher time-resolution studies is Conrick and Mass (2019) who used 10 minutes data to evaluate the performance of a numerical weather prediction model WRF-ARW[2], in comparison with precipitation observations from one winter season. A detailed characterization was performed using the drop size distribution (DSD) of rainfall. The model was proven to realistically capture the liquid water content (LWC), while the median volume diameter was prone to overestimation.

I will move forward with the idea of examining high-resolution data for both observations and model output. The operational model in Norway will be used as the basis for the model comparison. A relatively new tool called diagnostics in horizontal domain (DDH; Météo-France, 2019) makes it possible to extract model data on every time step (75 seconds for AROME-MetCoOp (Bengtsson et al., 2017)). Detailed observational data sets of 1 minute resolution are available from the Geophysical Institute in Bergen. By using a time-resolution of 5 minutes, we can enable a direct comparison of precipitation observations and model output. This will make it possible to investigate how well the model really represents the complexity of the precipitation events.

I have focused my work towards the following two key research questions:

1. How can we characterize the precipitation in a way that make it possible to compare high-resolution observations and model data?
2. How does AROME-MetCoOp perform compared to high-resolution observations of precipitation?

The precipitation characterization needs to be executed using parameters obtainable from both observation and model output. Based on the approach of Conrick and Mass

[2]The Weather Research and Forecasting model (WRF) with the Advanced Researcher (ARW) solver.

(2019), I have chosen to use the drop size distribution as the basis for characterizing the microstructure of the rainfall. From weighted moments of the DSD we can derive other integral rainfall parameters of interest (Testud et al., 2000). A combination of three parameters, the liquid water content (LWC), the mass weighted mean volume diameter (mean volume diameter, D_m) and the normalized intercept parameter (N_0^*) give a comprehensive description of the precipitation event. An advantage with this type of characterization is the possibility to calculate the exact same parameters (based on a different methodology) from the model output, as a basis for an accurate, direct comparison.

I also provide an example for how the methodology may be used, by comparing the observational data from the Geophysical Institute in Bergen to the model output from AROME-MetCoOp for a high-intensity precipitation event occurring over Vestlandet July 30^{th} 2019. The model comparison has been performed using both spatial and point validation. Clear differences was seen between the observations and the model. Providing important knowledge of where the model face challenges.

All studies with model prediction, works to contribute to a better understanding of the model and its limitations. They all want to help in the model development. The goal is to achieve the best possible model representation of every weather situation. The chaotic behaviour of the atmosphere makes a perfect forecast impossible. However, new implementations are constantly made and the models are continuously improving.

I have focused my work on high-intensity precipitation, but the methodology can be applied to all types of future rainfall events. Further additions can be made in what type of parameters are included in the characterization and thus make it possible to asses forecast performance for all types of events. Being able to identify patterns of model deficiencies compared to observed events will hopefully lead to a more detailed understanding on how different precipitation events unfold in the model. Improved prediction of precipitation will give more accurate information of time, location and intensity for extreme events. This will again increase the possibility for better preparations and limit the consequnces.

The thesis is structured into five main sections. A detailed description of the data and methodology needed for enabling the comparison is described in section 2. This is followed by section 3 where I provide an example event taking the methodology in use. A discussion of my results is available in section 4 and lastly, I summaries the findings and give a future outlook in section 5.

2 Data and Method

Precipitation will be the focus during the comparison, but the variables provided by the instrumentation and the model varies. For this thesis, I have developed a methodology for enabling a direct comparison of high-resolution observations with model data from the operational weather forecast system AROME-MetCoOp (Müller et al., 2017). The methodology derived for each precipitation parameter used in this thesis: rain rate, liquid water content, mean volume diameter, normalized intercept parameter, and terminal fall velocity, are explained in detail in section 2.4

In this chapter I will first describe the different measurement instruments, then provide a description of the model and finally explain the methodology necessary to make a comparison possible.

2.1 Observational Data

The basis of the observational data are four ground based instruments permanently located at the Geophysical Institute in Bergen. The Automatic Weather Station (AWS), the TPS-3100 Hotplate Pluviometer (TPS), the Ott Parsivel^2 Disdrometer (from now on in the text: Parsivel) and the Micro Rain Radar Metek MRR-2 (MRR) are all measuring precipitation characteristics for a point location.

All four instruments apply different measuring techniques for precipitation. The result however, is precipitation measurements of 1 minute time resolution. A general description of each instrument will be provided in the following sections.

Three of the instruments the MRR, the TPS and Parsivel are located at the roof of the Geophysical Institute in Bergen (45 m a.s.l). While the automatic weather station is situated in front of the building at surface level.

2.1.1 The Micro Rain Radar MRR-2

The Micro Rain Radar MRR-2 (MRR, Metek GmbH, Germany) measures a series of precipitation parameters with a K-band doppler radar pointing vertically (METEK, 2009). Electromagnetic waves are sent out at a frequency of 24.23 GHz, and the back-scatter from hydrometeors are measured. From the back-scatter, the MRR provides information about rain rate, liquid water content, reflectivity and drop size distribution. The measurements are divided into 64 spectral bins of size and speed. The MRR has a high resolution sampling rate of 25 Hz, from which 10 seconds average profiles are made. The vertical range for the MRR at GFI was set to measure from 100 m up to 3100 m, with a level interval of 100 m. This can be adapted depending on measuring aim. Due to large surface backscatter the first two levels are discarded. Therefore, the first level of measurements is at 300 m above the MRR placement. This height difference is important to keep in mind for comparison with the other instruments.

2.1.2 The Ott Parsivel^2 Disdrometer

The Ott Hydromet particle size and velocity (Parsivel^2) Disdrometer is a laser optical disdrometer used to gather information about the drop size distribution of precipitation. A horizontal laser beam is sent out between two measuring houses. When drops fall through the light, the shape and length of time for the shadow of the drops is

used to determine the diameter and velocity (Raupach and Berne, 2015). The drops are then categorized into 32 bins for size (between 0-26 mm) and speed (0-22.4 ms^{-1}). The two smallest size classes are discarded due to low signal-to-noise ratio (Battaglia et al., 2010).It is also of importance to note that assumptions made during calculations in Parsivel^2 makes the instrument more suited for measuring rainfall compared to snow and graupel (Battaglia et al., 2010)

2.1.3 The TPS-3100 Hoplate Pluviometer

The TPS-3100 Hoplate Pluviometer (TPS) measures precipitation through the use of a heated aluminium disk. The disk consists of two heated, isolated plates where the upward facing plate captures precipitation. The precipitation is evaporated (and melted first in case of snow) by the heated disk. The precipitation rate is calculated from the power needed to keep the surface of the plate at constant temperature during the evaporation (YES, 2005). The downward facing plate is sheltered from the precipitation, and is therefore only affected by wind. This plate is therefore used as a reference plate to correct for wind cooling. The precipitation rate is proportional to the difference in power required to heat the top and the bottom plate (Rasmussen et al., 2011).

The precipitation rate (mm h^{-1}) is calculated for every minute. However the 5 minute average needs to exceed a 2 W threshold for the measurements to be registered as precipitation. The threshold takes into account the wind variations on the two plates and the diurnal radiation influence on the temperature (Rasmussen et al., 2011).

2.1.4 The Automatic Weather Station

The automatic weather station measure all the common weather parameters and is often used as a reference instrument. A combination of sensors placed on a mast give measurements of pressure, air temperature, relative humidity, wind direction and speed, radiation, and precipitation.

A Pessl IM523 rain gauge is used to measure precipitation. The rain gauge use a tipping bucket for gathering precipitation measurements, with a threshold of 0.2 mm for tipping. The maximum capacity for measurements is 12 mm/min. The instrument has an accuracy of $\pm$ 5 $\%$ of the measurement. Measurements are gathered every minute and can be stored in 1 minute, 10 minute or 1 hour interval (ITAS, 2005).

2.2 Model Data

To compare with the observational data, I used AROME-MetCoOp combined with the relatively new tool called diagnostics in horizontal domain (DDH) (Météo-France, 2019) DDH enables us to extract the model data for every time step on a user-defined subdomain. This allows for a detailed investigation of the model data.

2.2.1 The AROME-MetCoOp Model

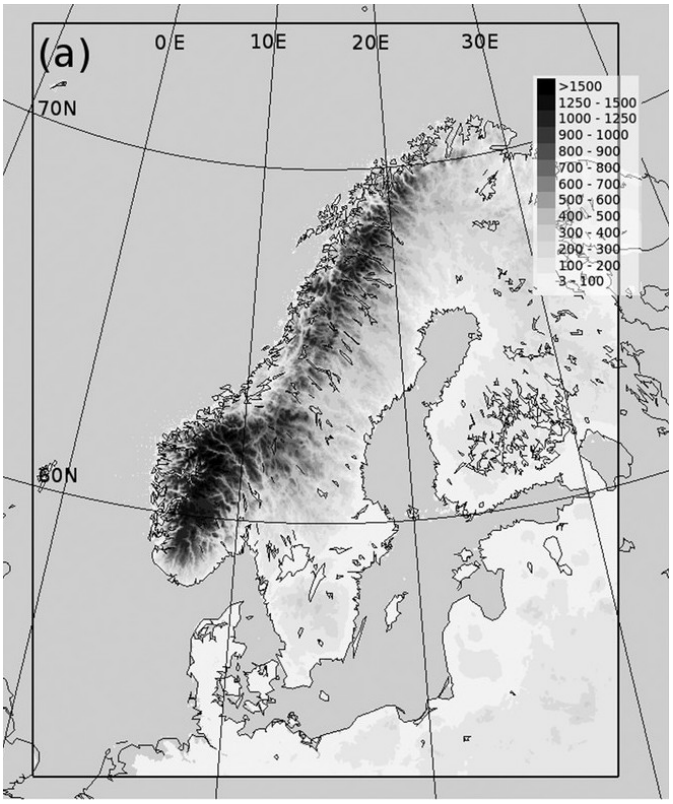

Figure 1: The full model domain for AROME-MetCoOp with land topography in contours (elevation (m)). Müller et al. (2017), Fig. 1.

AROME-MetCoOp is an operational, convection-permitting model run at the Meteorological Institute in Norway (Müller et al., 2017). The model domain includes both land and open water, and cover large parts of the Nordic countries and surrounding oceans (Figure 1) (Seity et al., 2011)). The model use a horizontal grid spacing of 2.5 km and 65 vertical levels. The levels are determined from a hybrid vertical discretization using mass and a terrain-following dependency.

AROME-MetCoOp is a non-hydrostatic model. The version, MetCoOp, is a further development of the french AROME model with a modified description of small-scale phenomena and forcing, better suited to Scandinavian conditions (Müller et al., 2017). Convective structures with a cloud depth exceeding 4000 m are fully resolved in the model dynamics (Kähnert et al., 2021). The smaller scales are still partly parameterised. For the operational simulations optimal interpolation is used for assimilation of surface variables. Three-dimensional variational data assimilation (3D-VAR) is used for the upper air assimilation. The boundary data is provided by the IFS-HRES model from

ECMWF (Seity et al., 2011). A semi-Lagrangian scheme is used for horizontal advection of the prognostic variables, while vertical advection of hydrometeors are done by a sedimentation scheme. Advanced parametrization schemes are in place for turbulence, surface, radiation, shallow convection and cloud microphysics. For the work in this, thesis the microphysical setup is the most important and will be closer described. Further information on the model configuration can be found in ((Seity et al., 2011),(Müller et al., 2017),(Méteo-France, 2009))

Microphysics
The microphysics scheme is mixed-phase. A Kessler scheme is in place for the warm processes. The originally three-class ice parameterization (ICE3) scheme for cold processes have been replaced by the OCND2 scheme, where cloud ice is parameterized by a cloud scheme instead of the large-scale condensation and thermodynamic adjustment scheme (Bengtsson et al., 2017). There are 6 resulting prognostic variables for precipitation. Namely the specific contents of water vapour, q_v, cloud water, q_c, rain water, q_r, snow, q_s, graupel, q_g, and cloud ice, q_i (Seity et al., 2011). There are more than 25 processes parameterized within the scheme and a lot of interaction between the different species (Müller et al., 2017). An overview of these processes can be seen in Figure 2. .

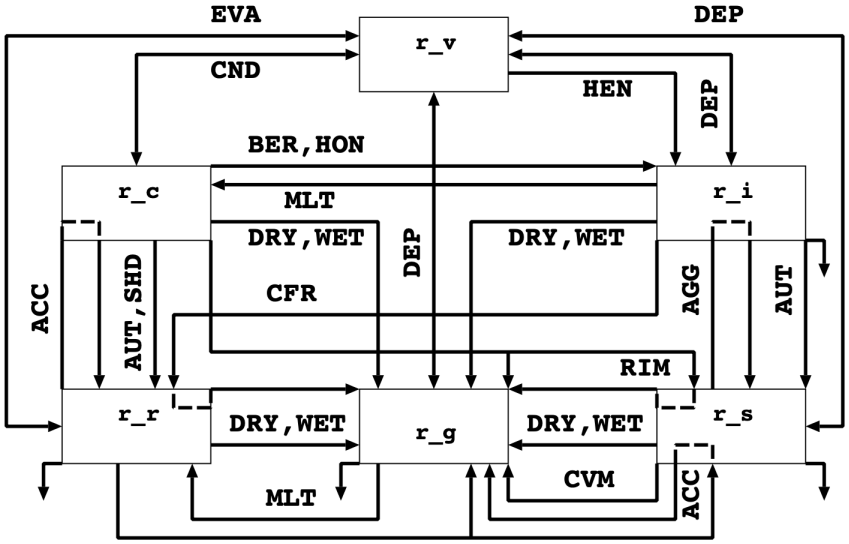

Figure 2: An overview of all the microphysical processes within the mixed phase scheme (Méteo-France, 2009, p.115).

In the microphysics scheme the water species are assumed to follow a generalized Gamma distribution for drop spectra, which is simplified to the exponential Marshall-Palmer distribution for precipitating species (rain water (q_r), snow (q_s), and graupel (q_g)) (Seity et al., 2011)

2.2.2 Diagnostics by Horizontal Domain

Diagnostics by Horizontal Domains (originally French, Diagnostics par Domaines Horizontaux, DDH) is a relatively new tool that can be used to extract prognostic variables

from numerical forecasting models on a user defined domain at every time step. DDH is currently available for three models: ARPEGE, ALADIN and all of the HARMONIE-AROME models (Météo-France, 2019).

DDH make it possible to obtain the tendency of the prognostic variables for every model time step for a A x A grid. For some processes, the default hourly output interval of the model is insufficient. In this thesis, DDH is used in combination with AROME-MetCoOp to obtain high-resolution data for a chosen domain around Bergen.

DDH has three different types of output domains that the user can define. The first two approaches use either a global domain or zonal bands, which both result in mean value output for the chosen domain. The third option, which is used in this thesis, is the user-defined sub-domain. Here, either singular grid points or a quadrilateral area is chosen. The approach using grid points will give high-resolution output for every chosen grid points, while choosing a quadrilateral area gives mean value output for the area.

In this work, 625 singular grids point were chosen, covering an area of 62.5 x 62.5 km (The domain is presented in Figure 7 in section 3.1 of the results). High-resolution data was extracted for every model grid point, at each model time step. The model simulation used from AROME-MetCoOp was initialized at 00 UTC on 30^{th} July 2019. In combination with DDH, model output for every 75 seconds was extracted for each grid point in our chosen domain. We kept as close to the operational model setup as we could. We did not run the full 3D-VAR, due to the lack of access to observational data. In addition the model simulation was performed without spin up time for the model. The close setup to the operational model was desired to make the comparison with observations as close to the predicted forecast as possible. To make computations more feasible output parameters were limited compared to the full AROME-MetCoOp model simulation.

2.3 Drop Size Distribution

Formation of precipitation is a result of microphysical processes acting on water vapour in the atmosphere. The result of these processes are individual drop size distributions (DSD) for every precipitation event (Willis, 1984). The DSDs can provide detailed characterizations of the precipitation, since weighted moments of the DSD can be used to derive other integral rainfall parameters. A combination of three of these parameters are often used together to give a comprehensive description of the intensity, particle size and the intrinsic shape of a rainfall event (Testud et al., 2000)

The DSD generally follows a gamma distribution (Zagrodnik et al., 2018). The raindrop concentration per diameter, N(D) (mm^{-1} m^{-4}), can then be expressed as

$$N(D) = N_0 D^{\mu} \exp(-\Lambda D) \tag{1}$$

where N_0 is the intercept parameter ($m^{-3}cm^{-1-\mu}$), D is the diameter, μ is the shape parameter, and Λ is the slope.

Often, μ has been set to zero, resulting in the exponential distribution also known as the Marshall-Palmer distribution (Marshall and Palmer, 1948).

$$N(D) = N_0 e^{-\Lambda D} \tag{2}$$

$$\Lambda = 41 R^{-0.21}\ cm^{-1} \tag{3}$$

where N_0 is set to a constant, $8 \cdot 10^6$ m^{-4} and R is the rain rate (mm h^{-1}).

The Marshall-Palmer distribution is often the assumed distribution in numerical weather prediction models, as seen for the precipitating species in AROME-MetCoOp.

In the characterization of the precipitation event occurring on 30^{th} July 2019 that I present below, I will use three parameters: liquid water content (LWC), mean volume diameter (D_m), and the normalized intercept parameter (N_0^*). Each parameter and the calculations necessary for the comparison of observations and model data are described in closer detail in section 2.4.

It is worth noting that the median volume diameter (D_0) traditionally has been the most used parameter for describing particle size in context with the DSD. However, several studies have shown the mean volume diameter to be a good approximation of the median volume diameter in most precipitation situations ((Wen et al., 2016) and (Testud et al., 2000)) The mean volume diameter has the advantage of beeing much easier to obtain for observational data compared to the median volume diameter. In addition, D_m can also be calculated for the model data used in this thesis, making a comparison possible.

2.4 Metrics for quantifying the precipitation parameters

To enable a direct comparison between instrument data and model data some data analysis is required. In this section, I explain the calculations and concepts behind the comparison methodology, but first a quick summary of the approach. We initially start with two different sets of data. Observational data and model prediction data. These provide different time resolutions and different output variables. In order to make a comparison between these two data sets, we first have to perform an extensive analysis on the individual data set. This is done through the metrics derived in this section. As a result, we will end up with similar characteristics for both model and observations, which we can use in a comparison.

First of all, a common time resolution needs to be established for the comparison. The instruments report data with a time resolution of 1 minute, while the AROME-MetCoOp model use a time step of 75 seconds. Throughout this thesis, I will therefore use time intervals of 5 minutes accumulated data or averaged data as a basis for comparison.

2.4.1 Rain Rate

Precipitation intensity is most commonly studied through accumulated rain rate for a defined period. Since rain rate is provided as an output variable in all 4 instruments, the accumulated 5 minutes rain rate (mm $5min^{-1}$) has been calculated for each instrument.

The DDH model output however does not directly provide rain rate. Therefore, the rain water (q_r) in the atmosphere has to be used as an indication for rain rate. Since

not all the available rain water will fall as precipitation, we first need to make an assumption from which level the precipitation will start. This can be done through the relation between speed and time resulting in distance. The mean terminal fall velocity of the drops calculated from the MRR, is about 5.3 m s^{-1}. The model time step is 75 seconds. This provides a distance of 398 m, which we can assume is the level where the rain water will fall as precipitation. There is of course an uncertainty to this approach for choosing a starting level for precipitation. The measured terminal fall velocity has uncertainties from the instrument accuracy. Drop sizes is not necessary the same in the model as in the observed precipitation, and may fall with a different speed. In addition, other meteorological conditions, for example wind, can affect the drops on their way down. The uncertainty will be further discussed in section 4.

Based on this calculation, I have calculated total precipitation water from the surface and up to 400 m (model level 52). If we assume no evaporation of rain water, this is the amount of rain water in the atmosphere we assume will fall to the ground as precipitation.

The formula for total precipitation water, TPW (m)

$$\text{TPW} = \frac{1}{\rho_w g} \sum_{n=0}^{n_i} q_i \, \Delta p_i \tag{4}$$

where ρ_w is the density of water, q_i is the mixing ratio of water vapor (kg kg^{-1}) and dp_i is the pressure difference between each model level, i.

2.4.2 Liquid water content

Another way to examine the rain intensity is through the liquid water content (LWC, g m^{-3}). LWC is a measurement for the amount of liquid water available in the atmospheric column above a unit area. LWC can be calculated from the third moment of the drop size distribution as

$$\text{LWC} = \frac{\pi \rho_w}{6} \int_0^\infty N(D) D^3 dD \tag{5}$$

where N(D) is the number concentration of droplets per diameter class per unit volume ($mm^{-1}m^{-4}$), D is the diameter of the droplets (m) and ρ_w is the density of water (g m^{-3}) (Testud et al., 2000).

LWC is provided as an output variable in the MRR. For the Parsivel it need to be calculated.

Liquid water content also needs to be calculated for the model. However, the model output does not have number concentration as a prognostic variable. We therefore base the calculation for LWC in the model on the mixing ratio of rain water (r_r) and liquid cloud water(r_l), through the formula

$$\text{LWC} = \sum_{n=0}^{64} \rho_m (r_r + r_l) \tag{6}$$

where ρ_m is the density of each model level.

The DDH data does not provide density. Therefore, density was calculated from the equation for hydrostatic balance.

$$\frac{dP}{dz} = \rho_w \, g \tag{7}$$

where p is the pressure, z is the height, ρ is the density and g is the acceleration of gravity.

2.4.3 Mean volume diameter

The mean volume diameter (D_m) representative here as a parameter describing drop size in the precipitation. D_m can be obtained using the relation between the fourth and third moment of the drop size distribution (Testud et al., 2000)

$$D_m = \frac{\int_0^\infty N(D) D^4 dD}{\int_0^\infty N(D) D^3 dD} \tag{8}$$

The Parsivel provides the mean volume diameter an output variable. For the MRR data, D_m needs to be calculated.

Again, the model does not have any size variables. Therefore, a power law relationship is used to link the particle diameter to mass and terminal fall velocity (Seity et al., 2011) The D_m can then be obtained from

$$D_m = \left(\frac{V_T}{a \left(\frac{\rho_{00}}{\rho_{dref}} \right)^\alpha} \right)^{\frac{1}{b}} \tag{9}$$

where V_T is terminal fall velocity of the drops, ρ_{00} is air density at a reference pressure P_{00}, ρ_{dref} is a reference pressure and a, b, and α are constants with values 842 $m^{0.2} s^{-1}$, 0.8, and 0.4 respectively (Méteo-France, 2009)

Terminal fall velocity is further described in chapter 2.4.5.

2.4.4 Normalized Intercept parameter

The intrinsic shape can be expressed through another parameter obtainable from the DSD, the normalized intercept parameter N_w (mm^{-1} m^{-3}). The intercept parameter gives the raindrop concentration (mm^{-1} m^{-3}) (Huang et al., 2021). For a gamma-shaped DSD, the intercept parameter can be expressed from LWC and median volume diameter (Thompson et al., 2015).

$$N_w = \frac{3.67^4 10^3}{\pi \rho_w} \frac{LWC}{D_0^4} \tag{10}$$

However the intercept parameter can also be expressed using the mean volume diameter (Testud et al., 2000).

$$N_0^* = \frac{4^4}{\pi \rho_w} \frac{LWC}{D_m^4} \tag{11}$$

In this case, the same equation (11) can be used to calculate the intercept parameter for both instruments and the model.

2.4.5 Terminal Fall velocity

The terminal fall velocity V_T (m s^{-1}) of a drop is the constant speed at which the drop falls when drag force and gravity are in balance. V_T can be calculated from the first moment of the DSD (METEK, 2009).

The terminal fall velocity is a parameter of interest when describing a precipitation event in the vertical. The parameter is given directly from the MRR. However, this is not the case for the model output. In that case, the relation between the drop diameter and mass can be applied to calculate the terminal fall velocity.

For a raindrop with diameter D, the terminal fall velocity can be calculated from

$$V(D) = \left(\frac{\rho_{00}}{\rho_{dref}}\right)^{\alpha} aD^b \tag{12}$$

here, α = 0.4, a = 842 $m^{0.2}$ s^{-1} and b = 0.8.
We can calculate the terminal fall velocity for every droplet diameter in the rainfall using

$$V_T \rho_{dref} r_r = \int_0^{\infty} \frac{\pi}{6} \rho_{lw} D^3 V(D) N(D) dD \tag{13}$$

where ρ_{00} is air density at a reference pressure P_{00}, ρ_{pdref} is a reference density, and ρ_{lw} is density of water (Méteo-France, 2009). From this we can get the equation:

$$V_T = \frac{a}{6} \Gamma(b+4) \left(\frac{\rho_{00}}{\rho_{dref}}\right)^{\alpha} \left(\frac{\rho_{dref} r_r}{\pi \rho_{lw} N_0}\right)^{\frac{b}{4}} \tag{14}$$

Since the output data from DDH does not give droplet diameter I will use eq. 14 to calculate the terminal fall velocity for the model grid points.

3 30^{th} July 2019 - An Example for the Comparison Methods

3.1 The General Weather Situation 30^{th} July 2019

I have now derived a methodology for enabling a direct comparison of high-resolution precipitation observations with the output from the operational weather prediction model. I will now demonstrate the usefulness of this methodology through an example, using one high intensity precipitation event from the 30^{th} July 2019.

The event occurred over large parts of Vestlandet on July 30^{th} 2019. Bergen was chosen as location for this comparison due to the detailed observational data set available from the instruments at GFI.

The event moved in over Vestlandet during the afternoon on Tuesday the 30^{th} of July and lasted until midday the next day. The highest intensity precipitation occurred early in the event. I have therefore defined an event period for the comparison from 15:00-23:00 UTC in order to limit the amount of data necessary for the model run. The precipitation occurring after 23:00 UTC was similar to the last hours of the defined event time.

As stated in the methodology, a time-resolution of 5 minutes is needed for the direct comparison between observations and model output. From now on, times stated in the text will use the time for the start of the interval. For example, the time interval between 15:00-15:05 will be written as 15:00. All times are given in UTC.

I will start by presenting the large-scale general weather situation for the day. Then I shift focus to precipitation and the characterization of this precipitation.

3.1.1 The Large-Scale Situation

An overview of the weather situation for 30^{th} July 2019, 18 UTC, is presented in a synoptic weather analysis chart from the Meteorological Institute in Norway (Figure 3) (Meteorologisk Institutt, 2019).

A high pressure system was present in the Norwegian sea, while low pressure systems were located to the south and east of Norway. The previous week was dominated by warm air masses situated over southern Norway (Meteorologisk Institutt, 2019). During the afternoon on July 30^{th}, colder air masses moved in from east/north-east over the mountains. The passage provided access to large volumes of moist air, providing the necessary conditions for heavy showers and thunderstorms.

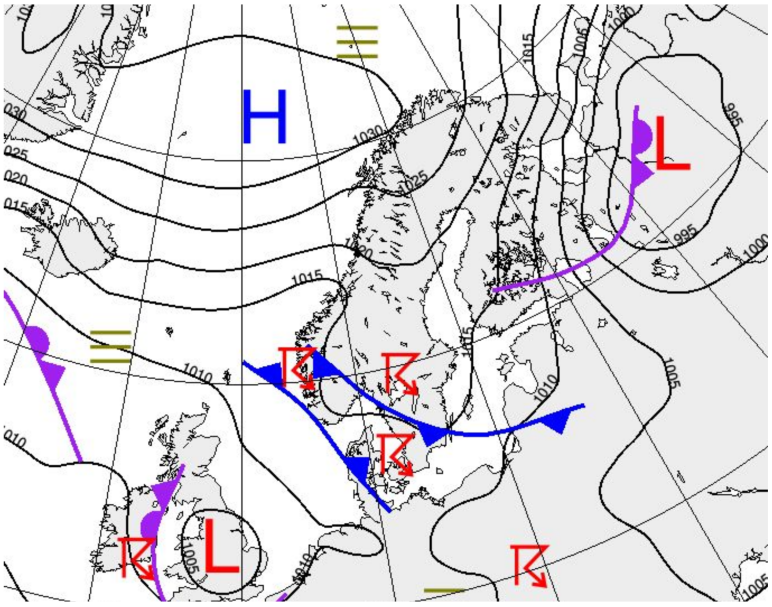

Figure 3: Synoptic weather analysis chart over northern Europe for the 30^{th} July 2019, 18:00 UTC. Presenting the pressure and frontal situations, and warnings for fog and thunder. Obtained from the Meteorological Institute in Norway (Meteorologisk Institutt) (Meteorologisk Institutt, 2019).

Situations where moist air masses move in from the east over the mountain is relatively uncommon for Bergen. Most often, precipitation is a result of warm, moist air from the North Sea, moving in from west/south-west over the coast of Norway resulting in lifting and condensation.

From three snapshots taken at 00:00 UTC Figure 4 a), 12:00 UTC (Figure 4 b) and 23:00 UTC Figure 4 c) we can see the evolution of the predicted liquid water content transport (TCL) and ice water content transport (TCI). This clearly shows that the model also captures the direction of the moisture moving in over the mountains.
Also visible is the high-pressure system located in the Norwegian sea, same as for the weather chart (Figure 3). And the low-pressure systems located to the east of Norway and to the south of Norway.

3.1.2 Precipitation

To be able to evaluate differences between predicted precipitation and observed precipitation, it is important to quantify differences between different measurement methods first.

Observed Precipitation
The resulting precipitation from the incoming moisture discussed above can be seen in the observational chart for the accumulated precipitation around Bergen (Figure 5). The area containing Bergen obtained the most precipitation, between 40-60 mm during a 24 hour period, while surrounding areas experienced precipitation amounts up 20-40 mm for the same period.

Zooming in on a point location for Bergen, we get an overview of intensity, intermit-

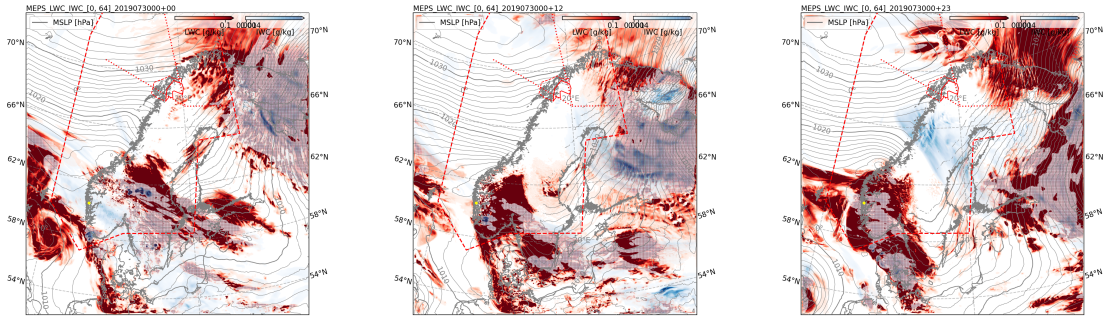

(a) 00:00 UTC (b) 12:00 UTC (c) 23:00 UTC

Figure 4: The cloud water situation for 30^{th} July 2019. Liquid water content (red shading) and ice water content (blue shading). Model simulation started on 30^{th} July 2019 00 UTC. The evolution of the cloud water situation are shown for valid times (a) 00:00 UTC, (b) 12:00 UTC and (c) 23:00 UTC. Note: the legends are misslabeld, should be TCL and TCI (g m^{-2})

tence and amount of precipitation occurring during the event by studying the rain rate (Figure 6).

Precipitation is first registered by the MRR (indigo line) in the time interval between 16:25-16:30. The precipitation is continuous during the whole event period, with various intensity. The rain rate is weak in the first 10 minutes, before high intensity rainfall occur. Two main peaks are present in the rain intensity. The first peak occur at 16:45 and includes the maximum rain rate intensity of 2.8 mm $5min^{-1}$. The second peak at 17:10 is weaker with intensity of 2.1 mm $5min^{-1}$. In the time following both peaks, the precipitation calms down, before slightly increasing again.

Overall, the other three instruments are in relatively close agreement with the MRR. The Parsivel^2 (red line) has a similar time evolution, though it appears to be shifted 5 minutes later compared to the MRR. The rain rates are overall lower, with a maximum intensity of 1.8 mm $5min^{-1}$.

The AWS (blue bars) together with the TPS (orange bars) register the latest start of precipitation, at 16:40. Again, the evolution is similar to the two other instruments, but intensity varies. The AWS measurements are in general lower than those from the MRR, but higher than the Ott Parsivel^2 and the TPS. The rain rate maximum is measured to 2.4 mm $5min^{-1}$. After 19:00, the rain rate calms down to intensity below the AWS tipping threshold of 0.2 mm and precipitation is only registered for certain intervals. The TPS are also in general agreement with the evolution of the rain rate, but shifted a bit to the right. A comparison between the TPS and the Ott Parsivel^2 show a 2 minute time shift for the registered drop in temperature before the start of the precipitation (figure not shown). The TPS registers the latest maximum intensity of 2.0 mm $5min^{-1}$ at 17:00.

In summary, all instruments display a similar continuous two peaks rain rate evolution. The time and intensity of rain rate however have small variations. The high intensity period have the largest difference with a maximum offset of about 1.5 mm $5min^{-1}$. During this period of time the MRR in general have the highest values, while Parsivel have the lowest. The instruments are in closer agreement in the following calmer pe-

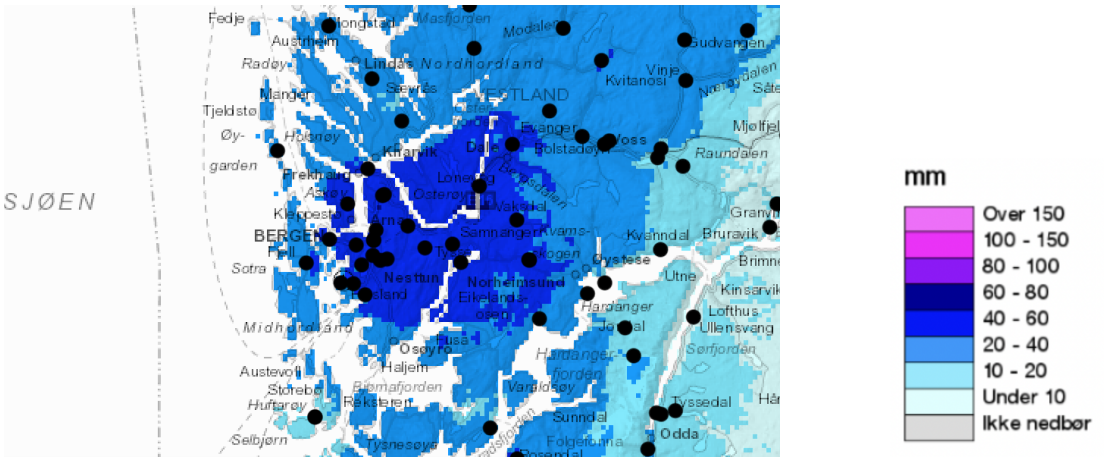

(a) (b)

Figure 5: Accumulated precipitation for 30^{th} July 2019, in the area around Bergen. Precipitation accumulated over 24 hours between (shadings) and observational stations (black dots). (Taken from SeNorge)

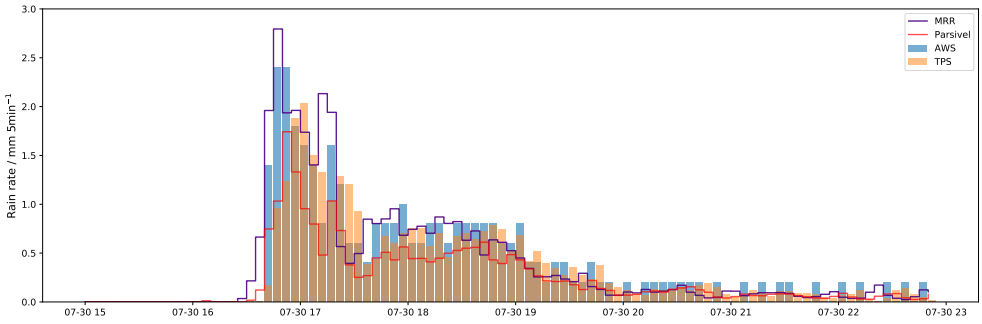

Figure 6: Time series of the 5 minutes accumulated rain rate (mm $5min^{-1}$) on 30^{th} July 2019 from 15:00-23:00 UTC. Presented for the MRR (indigo line), the Ott^2 parsivel disdrometer (red line), the AWS (blue bars), and the TPS (orange bars).

riod. The implications of these findings will be further discussed in section 4.

Predicted Precipitation

The model predicted accumulated precipitation for the defined event, in the study area shown for each grid point, gives an overview of the spatial variation in the chosen model domain (Figure 7). For comparison, the observed accumulated precipitation at GFI is also represented (circle). The value represent the mean accumulated precipitation for all the four instruments. With a value of 31.8 mm $8h^{-1}$ the observations register more precipitation compared to the model prediction of 23.8 mm $8h^{-1}$ in this location.

I will move forward with 6 grid points for the comparison. Each model grid point has been given a reference name (Table 1). The name represents the nearest surrounding place. First is the point Florida, which is the grid point geographically representing the location of the instruments. Second is a mean of all neighbour points centered around Florida. The mean is taken for the 9 grid points: (13,12), (14,12), (15,12), (13,13), (14,13),

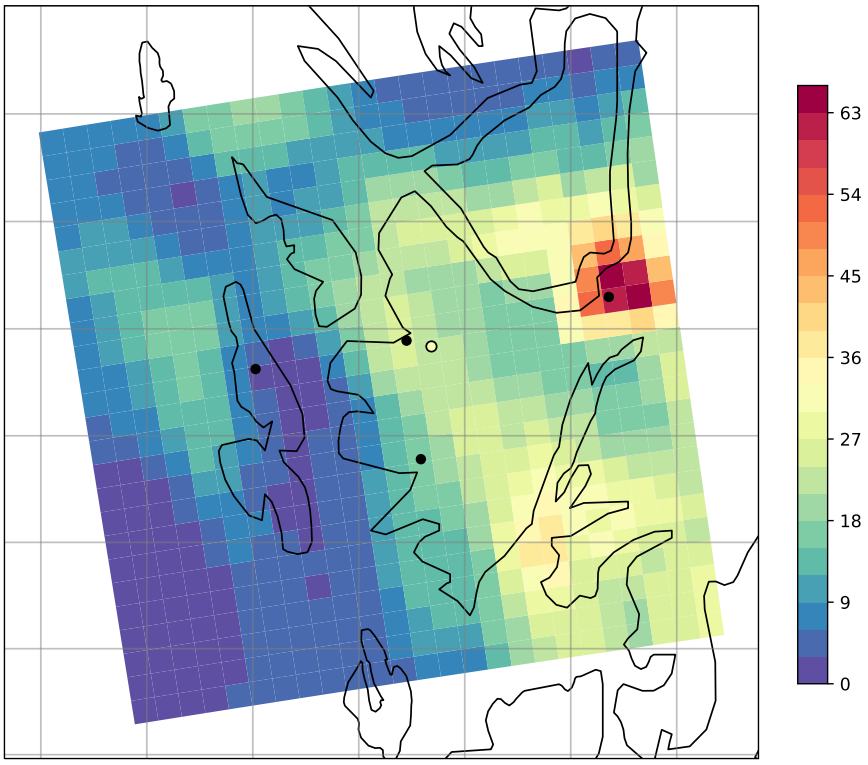

Figure 7: The predicted accumulated precipitation in the DDH output domain for the period between 15:00-23:00. The model predicted precipitation for each grid point (shadings, mm $8h^{-1}$) are compared to the observed precipitation in Florida (circle).

(15,13), (13,14), (14,14), and (15,14). Third point, Hordnesskogen, represents the point closest in shape of the rain rate evolution and starting point to the observations. Fourth point, Laksevåg, have a similar accumulated value to the observations. Fifth point, Trengereid, have the closest maximum rain rate to the observations. And the sixth point, Skålvik, represent a point on the west side, experiencing less precipitation.

There is quite some variation in the amount of precipitation within the domain. In general, there is more precipitation on the east side of the domain, seen in the points for Trengereid, Florida, Laksevåg and Hornesskogen (Table 1) . The maximum amount of rain over the 8 hour period is 64 mm measured in point (22,15) and (23,14). While several areas on the west side experience no precipitation. The accumulated precipitation predicted for the grid point representing Florida (14,13) was 23.8 mm $8h^{-1}$. This is in the lower range of the measured precipitation from the instruments (ranging from 22.9-36.5 mm $8h^{-1}$). Thus, the accumulated values of precipitation for Florida is above the values registered for Parsivel[2].

We now shift our focus to a higher time-resolution of 5 minutes. The maximum rain

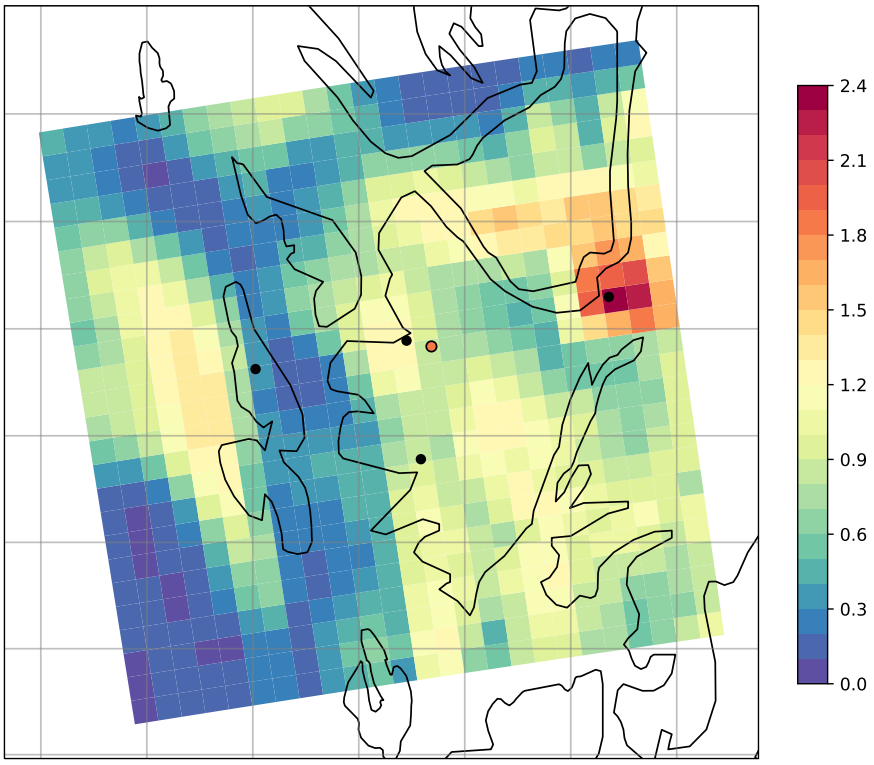

Figure 8: The maximum predicted rain rate in the DDH output domain for the period between 15:00-23:00. The model predicted rain rate for each grid point (shadings, mm 5min^{-1}) are compared to the maximum observed rain rate from the observational mean in Florida (coloured circle). Grid points of further interest for the comparison is shown in black.

rate (mm 5min^{-1}) for each model grid point show a similar variability as the accumulated rainfall (Figure 8). Model point Florida have much lower values compared to the maximum intensity of the observational mean. The only area reaching up to the intensity of the observational mean, is the points around Trengereid, east in the domain.

From the spatial variation of accumulated precipitation and maximum rain rate in the model, several grid points of interest have been chosen for further comparison with the observations (Table 1). An animation of the predicted precipitation event will be added to the thesis. This is just meant as a supplement for understanding the spatial variability and the development of the precipitation in the model.

Now we move forward with our 6 grid points of interest and investigate the evolution of rain rate on a higher time-resolution of 5 minutes (Figure 9).

Table 1: The coordinates of the model grid points used for comparison, and the a location reference name assigned to these.

N	Coordinate of model grid point	Reference name
1	(14,13)	Florida
2	Mean of the 9 neighbour grid points with Florida in center	Neighbour points
3	(13,9)	Hordnesskogen
4	(13,14)	Laksevåg
5	(22,14)	Trengereid
6	(7,13)	Skålvik

Precipitation first occur in the north-east of the model domain around Trengereid. The event start with one precipitating cell, providing intense rain rates, with a maximum of 2.4 mm 5min^{-1}, before it move east, out of the domain (see animation). Later in the evening a band of precipitating cells move in from the south, covering larger parts of the domain. Precipitation arrived in all our chosen grid points, but the evolution varied. The precipitation was weaker compared to the first cell, however it intensifies in certain areas. Again, a higher rain rate in Trengereid occur, and we assume that this enhanced precipitation is a topographic feature in the area.

Hordnesskogen, Laksevåg and Florida are all affected by the same precipitating cell coming in south in the domain (Figure 9). The cell first reached Hordnesskogen, with a maximum intensity of 0.9 mm 5min^{-1}. The band strengthens in intensity at the points (13,13), (13,14), and (13,15). They all have a similar evolution and is represented here by Laksevåg, with a maximum rain rate of 1.3 mm 5min^{-1}.

Hordnesskogen is further south compared to the others, and first affected by the precipitation cells. Precipitation start at approximately the same time as the observed precipitation and a similar evolution is visible (Figure 9). High intensity precipitation occur in the beginning, before calming down in the evening. However the intensity of the precipitation is weaker (maximum of 0.9 mm 5min^{-1}) compared to the observed strength of 2 mm 5min^{-1}. In addition the evolution is more compressed in the model. The high intensity precipitation last shorter, and is missing the two peak evolution that is present in the observations. The accumulated precipitation is 16 mm over the 8 hour period.

Precipitation starts at 17:00 in Florida, which is later compared to the observed precipitation start. From 17:40 and outward, the rain rate corresponds very well with the observations, only showing small variations. However, the first high intensity period in the beginning is completely missing from the model prediction.

This first peak is however present in Laksevåg, shifted one point to the north-west in the model domain. The peak starts later and increases slower in the model, and does not quite reach the strength of the observational mean, but there is more similarity to the evolution of the observational mean. The maximum intensity of 1.3 mm 5min^{-1} is also relatively close to the maximum for Parsivel (1.75 mm 5min^{-1}), when comparing to the individual instruments. However, also here, there is only one peak in the high intensity precipitation. The second period of enhanced precipitation fits in intensity around 0.8 mm 5min^{-1}, but the duration is shorter. Yet, the accumulated value

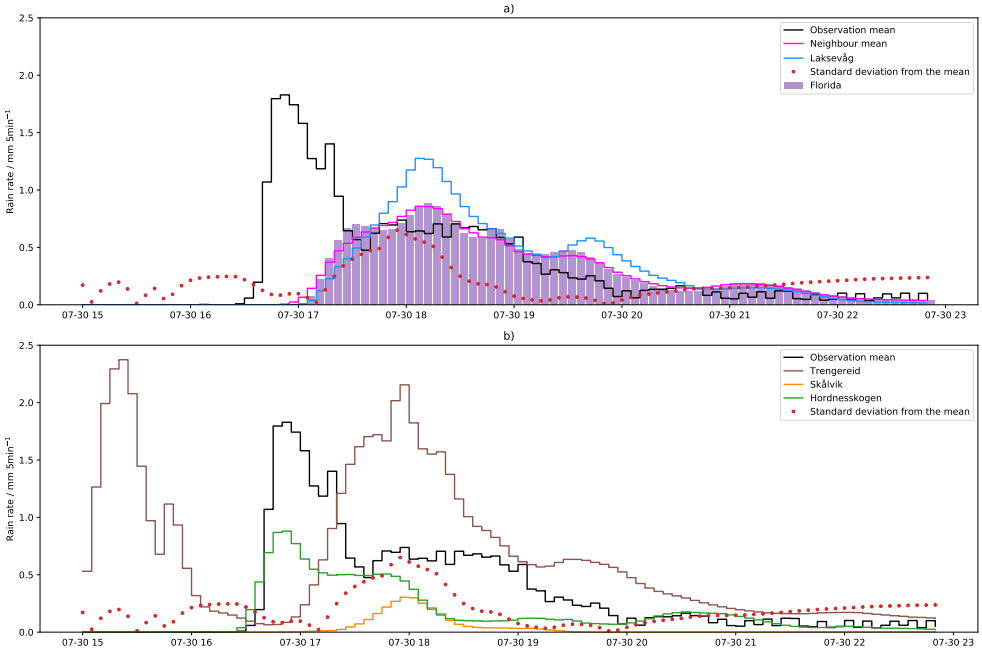

Figure 9: A comparison of observed and predicted accumulated 5 minutes rain rate (mm 5min^{-1}). The observational mean of the instruments (black line) is compared to a) the grid point representing Florida (purple bars) and the mean of all neighbour points with Florida as center (magenta line) and b) Trengereid (brown line), Skålvik (orange line), Hordnesskogen (green line), and Laksevåg (blue line). The standard deviation from the mean precipitation of the points is represented with a red dotted line.

of 27 mm 8 hours^{-1} is well within the range to the accumulated value of the observations.

The point furthest west in the domain only experience a short amount of precipitation for a short period of time. The accumulated precipitation is 2.8 mm over the 8 hour period, with a maximum intensity of 0.3 mm 5min^{-1}. Thus this is the point furthest apart in values and evolution compared to the observations.

In summary, there are a lot of spatial variation in the model. Some locations get the high intensity peak, or something resembling it, while other points are missing it completely. The accumulated amount of precipitation is also highly variable. Florida, Laksevåg and the mean of the neighbouring points are within the range of the observations. Trengereid experience much more precipitation compared to the observations and Hordnesskogen and Skålevik experience less. Thus, we see that location is important in the model.

3.2 One Level Characterization of the Precipitation Event

In the methodology I provided a way to enable the direct comparison between high-resolution precipitation observations with the AROME-MetCoOp output. In this section I will present an example for such a comparison by characterizing the precipitation event for the ground level. This is done through an examination of the parameters the liquid water content (LWC), the mean volume diameter (D_m) and the normalized intercept parameter (N_0^*). The observed event is described first, followed by the comparison between observations and model prediction.

For this comparison it is important to keep in mind that the lowest level, differ between the instruments, and between instrument and the model. MRR measurements are located at 345 m and Parsivel measurements at 45 m. The first model level is located at 11 m and represents mean values for the whole column down to the surface.

3.2.1 The Observed Precipitation Event

The combination of rainfall parameters used for the characterization of the observed event are derived from the weighted moments of the drop size distribution, as described in methodology 2.4 The DSD is available from two of the instruments at GFI, the MRR and the Parsivel^2. From the examination of the rain rate , we know that these are the two instruments furthest apart in rain rate intensity (Figure 6). So for further characterization of this event and a reliable comparison to the model data we want to make sure the difference in rain rate does not significantly impact the DSD.

I therefore start the characterization by examining the DSD from the instruments. That is, I use the mean number concentration of drops, N(D), (mm^{-1} m^{-3}) with respect to diameter (mm), calculated for the entire time of precipitation from 16:30-23:00 (Figure 10). The DSD of the instruments are in addition compared to the well-known Marshall-Palmer distribution for different rain rates (Marshall and Palmer, 1948). A concentration cutoff of 10^0 mm^{-1} m^{-3} has been used due to higher uncertainty for larger drop sizes (Wen et al., 2017).

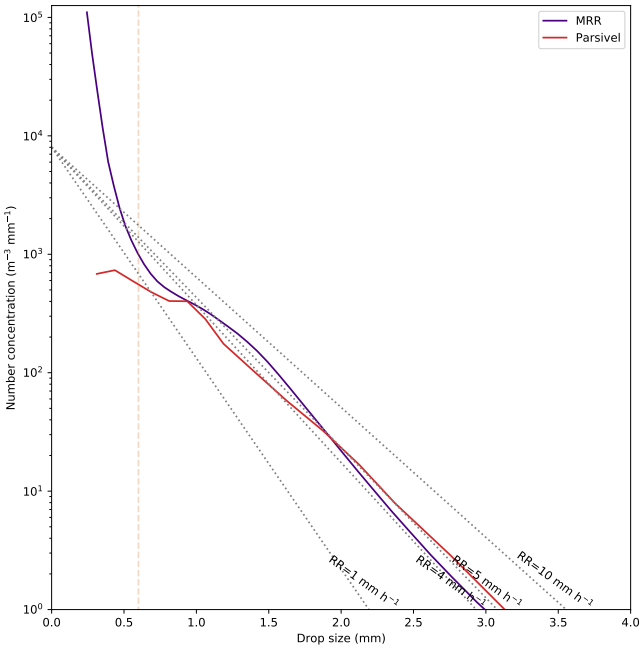

Figure 10: The mean drop size concentration (mm^{-1} m^{-3}) with respect to drop diameter (mm) for the time period 16:30-23:00. A comparison is made between the MRR (indigo line) and Parsivel[2] (red line). The Marshall-Palmer distribution is used as reference lines for four different rain rates: 1 mm h^{-1}, 4 mm h^{-1}, 5 mm h^{-1}, and 10 mm h^{-1} (grey dotted line). A cutoff for smaller drops is also shown (orange line).

A maximum concentration above 10^5 mm^{-1} m^{-3} is registered by the MRR (Figure 10, indigo line), for the smallest drop size 0.2425 mm. For drop sizes larger than 0.5 mm, the number concentration is substantially lower. The maximum diameter measured is 3.06 mm, when using the concentration cutoff. The DSD from the MRR does not directly follow one of the Marshall-Palmer reference distributions. However, from drop size 1.2 mm and up to 2 mm the decrease in concentration with size is close to the Marshall-Palmer distribution for rain rate 5 mm h^{-1}. Drops larger than 2 mm fit the rain rate distribution of 4 mm h^{-1}.

The DSD from the Parsivel is similar, but the concentration for the smallest drop sizes are substantially lower by a factor of 10^2 (Figure 10, red line). The maximum concentration of the Parsivel is registered for a larger diameter (0.437 mm) compared to the MRR. In addition, a larger maximum diameter of 3.25 mm is registered. The Parsivel follow the Marshall-Palmer reference lines in the opposite order compared to the MRR. Concentration decreases first following Marshall-Palmer distribution with rain rate 4 mm h^{-1} and then 5 mm h^{-1}. This means that the Parsivel in general has more of the larger drop sizes compared to the MRR, while the number of small and midsize drops are lower.

In conclusion the distributions of the two DSD are relatively similar despite the difference in rain rate and the measurement height difference. The largest uncertainty lies in the smallest drop sizes below 0.6 mm. This has also proven to be the case in previous studies (e.g Wen et al. (2017)) where the MRR has been shown to overestimate the number of small drops while Parsivel[2] has been prone to underestimation for

these size classes. In order to assure validity of this result shorter time intervals with averages over 5 minutes, 10 minutes and 1 hour have also been examined. The same conclusions could be drawn, and the longer time interval was chosen due to reduced noise level. For further interest is the study of the mean DSD for every hour available in the appendix.

Both instruments display DSDs approximately resembling the Marshall-Palmer distribution. There are deviations, especially for the small size classes, but the distributions overall are close to the exponential distribution.

Since this enhanced uncertainty with smaller and larger drop sizes is a known recurring problem for these instruments, we conclude that the difference in rain rate does not significantly impact the DSD in our case. Thus both instruments can be used for further characterization of the observed event. Nevertheless, it is important to keep in mind this uncertainty and I will use both the full drop spectra and a limited drop spectra during the further characterization of the observed event. As a consequence of the uncertainty, for the limited spectra, only drop sizes between 0.6-3.25 mm will be included, thus excluding the smallest and largest drop sizes.

3.2.2 .

The liquid water content

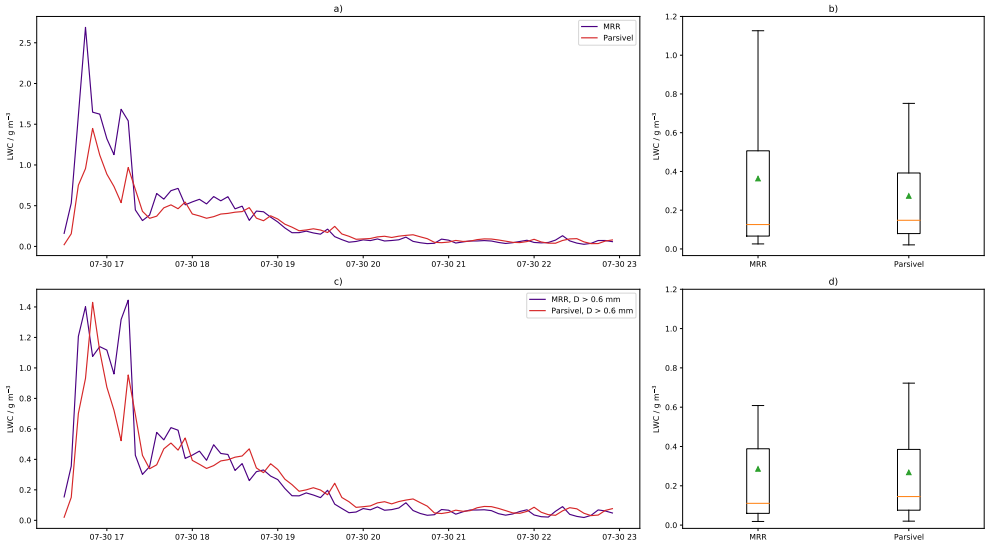

Figure 11: The observed liquid water content calculated for the period 16.30-23.00, for the MRR (indigo line) and Parsivel (red line). LWC calculated for all drop sizes are shown a) with a time series and b) with a box plot. In comparison the LWC calculated for drop size between 0.6-3.25 mm are shown in c) and d). The unit is given in g m^{-3}

The first parameter to compare observations and model precipitation characteristics is the liquid water content (Figure 11). The evolution of the LWC (Figure 11 a) shows two peaks in the amount of water present. Both peaks occur early in the precipitation period. The maximum peak of the MRR has a value of 2.7 g m^{-3}, while the second peak is weaker with values of 1.7 g m^{-3}. The amount of water is decreasing after both

peaks before slightly increasing again (same as for the rain rate). After 19:00 the LWC is stabilizing below 0.3 g m^{-3} with some intermittent lower values.

The LWC evolution for the Parsivel is very similar (Figure 11 a), red line). There is however a shift in time of approximately 5 minutes and the values are lower during the first 2 hours. This is especially noticeable during the first high intensity period, where the maximum of the Parsivel only reaches 1.4 g m^{-3}. When the precipitation calms down after 19:00, the values become closer to the values of the MRR. In addition, there are periods where the Parsivel has the higher values.

Next, I examine the statistical variability of the LWC (Figure 11 b). The median of the two instruments is almost equal, the MRR with 0.13 g m^{-3} and the Parsivel with 0.14 g m^{-3}. The lower end location of the interquartile range indicates the right-skeweness visible from the time series. Thus, the LWC for both instruments is dominated by lower values. The dispersion is larger for MRR, with values ranging from 0.1-0.5 g m^{-3}, while the total range of values almost reach 1.2 g m^{-3}. The spread of the Parsivel is more squeezed with values ranging from about 0.1-0.4 g m^{-3}. The maximum range reach almost 0.8 g m^{-3}.

The evolution of LWC changes when using the limited drop size spectra (Figure 11 c). The exclusion of the smallest drop sizes reduce the maximum peak for the MRR by approximately 1.3 g m^{-3}. The second peak however is only slightly reduced and now contain the maximum LWC, of 1.4 g m^{-3}. This indicates that the high concentration of small drops visible from the DSD greatly impact the start of the high intensity period of precipitation. However it is not the dominating factor for the second peak or for LWC at later times in the event.

The exclusion of the smallest drop sizes does not greatly impact the LWC of Parsivel. The evolution stays the same, as does the maximum amount of water. There is a slight reduction for some time intervals, but the small drops does not appear to be the dominating factor in the LWC of Parsivel. The agreement between the instruments is much closer compared to the full drop spectra calculations. The largest difference is now for the second peak, where MRR is about 0.4 g m^{-3} larger than the Parsivel.

The better agreement is also clear from the reduced dispersion of LWC for the MRR (Figure 11 d). The interquartile ranges from 0.1-0.4 g m^{-3}, about the same as for Parsivel. In addition, the Parsivel now has the largest overall spread. The median LWC of MRR also decreases slightly to 0.11 g m^{-3}, showing the general reduction in the amount of water available.

The predicted liquid water content

We start the comparison by examining the amount of water present for one level (Figure 12). Florida (Figure 12 a) shows no LWC before 17:00, meaning there is no rain water or cloud water present in the lower model level before this time. There is however some liquid cloud water present in the higher levels, (see section 3.3) The maximum peak from the observations is completely missing from the model at this point. Florida only shows a maximum LWC of 0.5 g m^{-3}, which means a difference of 0.9 g m^{-3} from the maximum observed LWC. However, from 17:20 and onwards the model captures the amount of water quite well. The fit between observations and model is indiscernible. There are some small variations, where the model slightly decreases while observations increase and opposite, but aside from this the LWC is well within the

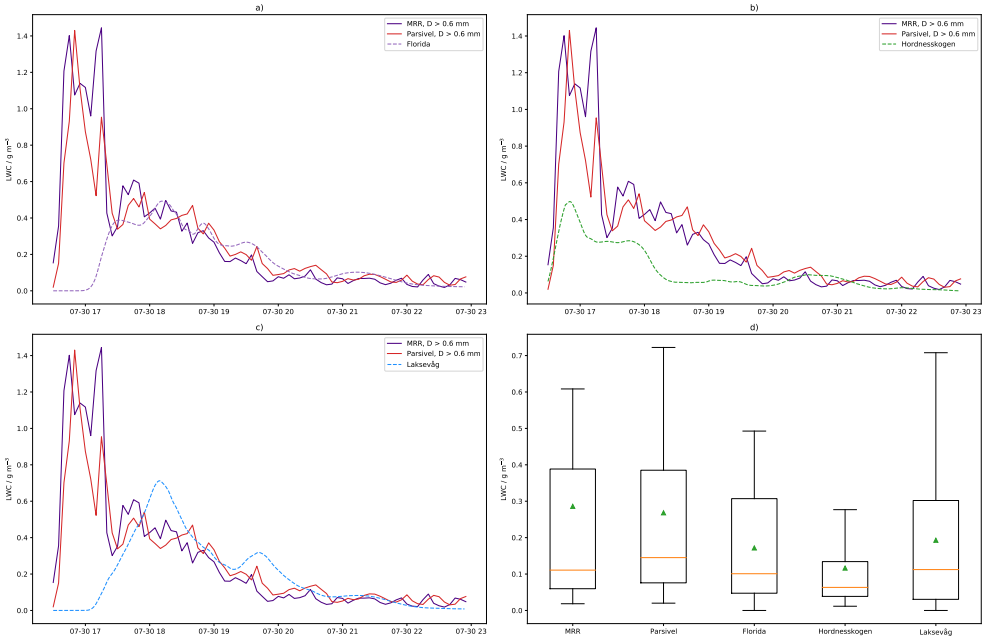

Figure 12: Comparison of LWC for observational data and the model prediction. The observed LWC for MRR (indigo line) and Parsivel (red line) is compared with the model point a) Florida (purple line), b) Hordnesskogen (green line) and c) Laksevåg (blue line). In panel d) a box plot displays the statistical variability for the entire event for both instruments and model points. Outliers are not included in the boxplot. Unit g m^{-3}.

range of each other.

If we are to take into account the whole time period of precipitation from the observations, Hordnesskogen has a more alike shape in evolution of the LWC (Figure 12 b). There is LWC present in the model from the same time as the observations. The maximum peak also occurs at the same time, with a decrease of LWC thereafter. However, the model does not capture the increase into a second peak, and the distribution is more compressed, with substantially lower values. The maximum LWC of the peak here also only reaches 0.5 g m^{-3}. It is only after 20:00 the model and the observations are in the same range.

Laksevåg (Figure 12 c) reaches closest to the maximum of the observations, with a value of 0.7 g m^{-3}. The distribution of LWC has a similar shape, however the time evolution is shifted by more than an hour later. In addition, the start has a much slower increase in LWC and the whole evolution is more compressed. Thus, compared to the other model points, Laksevåg has fewer times where the value is equal to the observations. There are only similar values for the time period around 19:00 and after 20:30.

The statistical variability for both observations and model grid points (except for point Hordnesskogen) is very close in the interquartile range with values between 0.031-0.388 g m^{-3} (Figure 12 d). The median values vary between 0.063-0.145 g m^{-3}, where Parsivel has the highest value and Laksevåg the lowest. Thus, the bulk of the LWC values are in the lower end of the scale. Hordnesskogen has less dispersion compared to the others, and the upper quartile only reaches 0.134 g m^{-3}, while the maximum

range is lower than the 75 percentile of the other points. The mean value of the LWC ranges between 0.116-0.286 g m^{-3}, whereby Hordnesskogen has the minimum and Laksevåg has the maximum.

The mean volume diameter

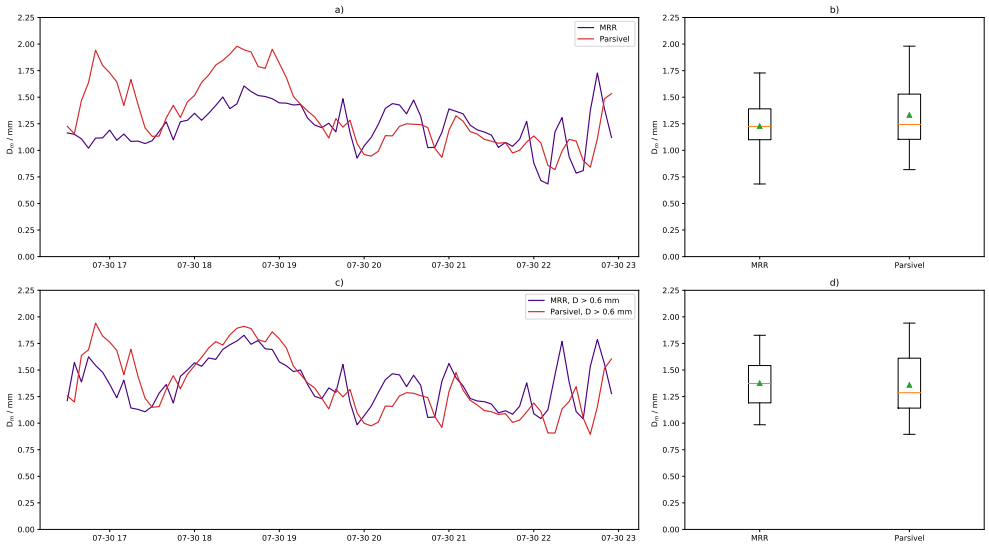

Figure 13: Same as Figure 11 for the mean volume diameter (mm).

A characterization of observed drop size is given through the mean volume diameter (Figure 13). For the full drop spectra the mean volume diameter of the MRR ranges between 0.68-1.73 mm (Figure 13 a), purple line). The start of the precipitation period shows a lower mean volume diameter compared to later times. This is the result of the large number concentration of small drops measured in the MRR during the high intensity period. After 18:00, the mean volume diameter increases, meaning that the domination of smaller drops decreases. However, the period shows more frequent fluctuations in the diameter size. The average mean volume diameter for the whole period is 1.23 mm.

The Parsivel has an opposite distribution compared to the MRR. The beginning of the event have the highest mean volume diameter, also including the maximum of 1.98 mm (Figure 13 a), red line). From the investigation of the DSD we could see that the concentration of smaller drops was not as pronounced in Parsivel. In addition larger drop sizes were measured, contributing to a larger mean volume diameter. The average over the whole period is also marginally larger, with size 1.33 mm. Later in the evening the diameter decreases and the distribution becomes more similar to the MRR.

From Figure 13 b) we can see that the distribution of diameter for the MRR is more symmetric compared to the LWC. The Parsivel distribution is still slightly skewed to the right, with a slightly larger mean volume median diameter. The Parsivel has a larger total spread in values, and the interquartile spread is also more dispersed.

The MRR in general gets a larger mean volume diameter, when using the limited drop spectra (Figure 13 c). The diameter in the beginning of the period increases, and becomes closer to the values of the Parsivel. The diameter for the Parsivel does not sig-

nificantly change. Thus, the evolution of the diameter between MRR and Parsivel is overall more equal. Especially the period between 18:00-19:30 is very alike. After 20:00 the differences are a bit larger, with the MRR showing higher values. The slight shift to the right in the Parsivel data is still present.

The exclusion of the small drops compresses the range of the MRR (Figure 13 d). The dispersion is now less for the MRR compared to the Parsivel data, and the overall range of the MRR is now contained within the Parsivel.The median of the MRR increases to 1.37 mm becoming larger than the median for the Parsivel (1.29 mm). Thus, the MRR diameter now have more larger values than the Parsivel. This provides a consistent observational .. for the comparison to the model data.

The predicted mean volume diameter

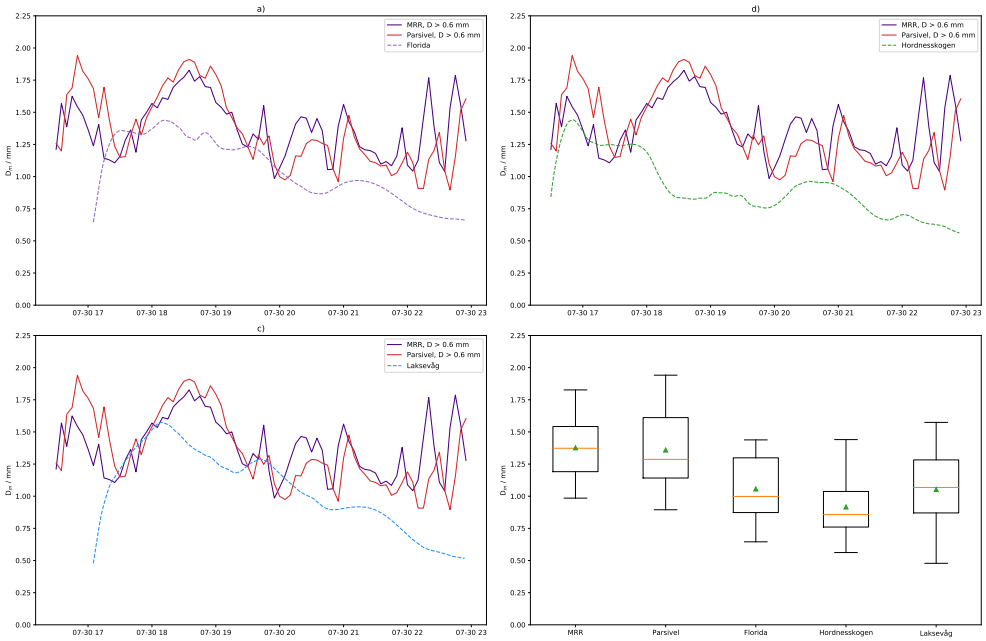

Figure 14: Same as for Figure 12, for the mean volume diameter (mm).

The mean volume diameter at Florida has in general lower values compared to the instruments (Figure 14 a). However, the shape of the evolution is similar most of the time. There is an increase in the beginning, and both observation and model have a period of increased diameter between 17:30-20:00. Florida has a maximum of 1.44 mm, 0.4-0.5 mm smaller than the MRR and the Parsivel respectively. After this time, the diameter decreases. The observations have a lot of fluctuations at this time. Some fluctuations are also present in the model, but not as frequent. The decrease is steadier in the model, reaching much smaller diameters.

The diameter of Hordnesskogen is overall lower compared to the observations, except for at the beginning of the event (Figure 14 b). The shape at the start of the preciptiation fits quite well, but we again see the faster evolving shape, making the maximum period decrease much sooner for the model. The shape after 20:00 however fits quite well with the observed diameter. The values are lower, but the fluctuations increase and decrease at the same time as the observations.

Closest in terms of values is Laksevåg (Figure 14 c)). It reaches a maximum of 1.57 mm, but also here the model shape is evolving faster than the observations. For two time periods, first between 17:15-18:10 and second between 19:30-20:00, the values align quite well with the observed mean volume diameter. Later in the evening the model has a more steady decrease compared to the observations. There are some fluctuations present, but they are a bit shifted.

The spread of the diameter is quite variable (Figure 14 d). All model points are shifted to lower values compared to the observations, the total spread does not reach up to the upper quartile of the observed values. Most shifted are the values for Hordnesskogen. This point also has the lowest median diameter of 0.86 mm and a mean value of 0.92 mm. The median diameter of Laksevåg is closest to the observations, while Florida has the closest mean value.

The normalized intercept parameter

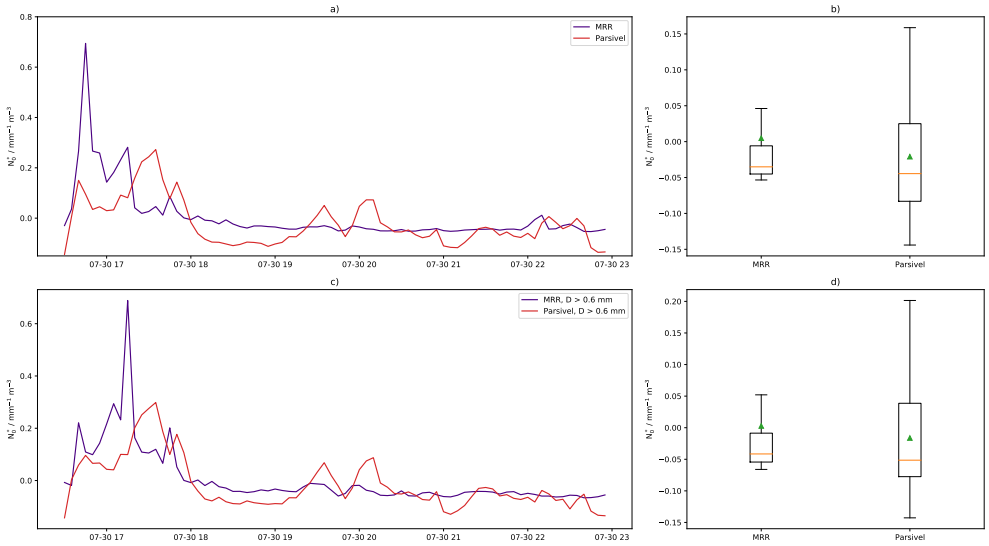

Figure 15: Same as Figure 11, but for the normalized intercept parameter N_0^* (mm^{-1} m^{-3})

For describing the intrinsic shape of the rainfall we examine the normalized intercept parameter N_0^* (Figure 15). The normalized raindrop number concentration with time shows the same two peak distribution for the MRR, as seen for the rain rate and the LWC (Figure 15 a). The maximum peak reaches a value of 0.7 mm^{-1} m^{-3}, at 16:40. This is followed by a rapid decrease to below 0.2 mm^{-1} m^{-3}, before it increases slightly again. After 18:00, the values stabilize below zero. The Parsivel has a weaker increase in the beginning, reaching the peak around 17:40. The maximum is weaker than for the MRR, with a value of 0.3 mm^{-1} m^{-3}. This is followed by a decrease to negative values. The Parsivel reaches stronger negative values than the MRR, and shows more fluctuations after 18:00.

When excluding the outliers, the normalized intercept parameter of the Parsivel is much more dispersed than for the MRR (Figure 15 b). The total range of the Parsivel is between -0.15-0.15 mm^{-1} m^{-3}, while the MRR stays between -0.05-0.05 mm^{-1} m^{-3}.

When using the limited drop spectra, the evolution of the MRR again changes (Figure 15 c). The maximum drop concentration is shifted closer in time to the maximum of the Parsivel. The mean normalized intercept parameter decreases from 0.005 to 0.003 mm^{-1} m^{-3}, meaning that the initial concentration of drops decreases. The Parsivel also experiences some smaller changes. The most noticeable is a shift in the median normalized drop concentration, becoming increasingly negative (Figure 15 c). Thus, the Parsivel data becomes more right-skewed. In addition, the total spread increases by 0.05 mm^{-1} m^{-3}. A slight increase in the total spread is also visible for the MRR,

In conclusion, excluding the smallest and largest drop sizes primarily affects the MRR measurements. The most noticeable changes are the reduction of LWC, the increase in mean volume diameter and the shift in maximum normalized raindrop concentration, all of which are occurring in the high intensity period. The Parsivel also shows some changes, but overall of much smaller impact.

When conducting the comparison between observations and model I will use the reduced drop size spectra. The reason for this is the larger uncertainty present for smaller drop sizes in the instrument measurements. Especially the very high number concentration registered for the smallest drop sizes in the MRR is of concern when including the full drop spectra.

The predicted normalized intercept parameter
The raindrop concentration is given through the normalized intercept parameter (Figure 16) . Precipitation first occur at 17:00 in Florida. The normalized intercept parameter (Figure 16 a) starts with a maximum value, at the same time as the peak for MRR, before rapidly decreasing to negative values in the same time as the peak for the Parsivel. Thereafter, weaker fluctuations are present. The parameter is normalized, so negative values in this context means that the concentration is below the mean value concentration. There is a perfect fit to the MRR between 18:00-19:00, while the Parsivel shows lower values, before increasing into two smaller, positive peaks. After 21:00, the model has positive values for the normalized intercept parameter, while the observations are negative. The evolution of Hordnesskogen differs significantly from the other model points. There is a small peak in the beginning, before values settles right below zero. There is however one longer period with a positive peak reaching up to 0.004 mm^{-1} m^{-3} in the time interval between 18:00-19:00. In this time, both instruments have a negative period. The normalized intercept parameter for Laksevåg is similar to Florida, however the negative values are more negative and the positive values are more positive.

All the model points are within the bounds of the observed values (Figure 16 d). However, the model is smaller, displaying a narrower range of values compared to the Parsivel. The MRR is closer in range of the model points. The Parsivel has the most negative median value, while Florida has the least negative value. The total dispersion of the Parsivel is the largest. This is due to the fact that outliers are removed, thereby the peak for MRR is not taken into account, and the Parsivel has a more uniform distribution. Hordnesskogen is the least dispersed, only varying between the minimum of -0.028 (mm^{-1} m^{-3} and the maximum of 0.004 mm^{-1} m^{-3}.

In summary, the model grid points are in general lower for all the compared rainfall parameters. However, all points capture different aspects of the observed event.

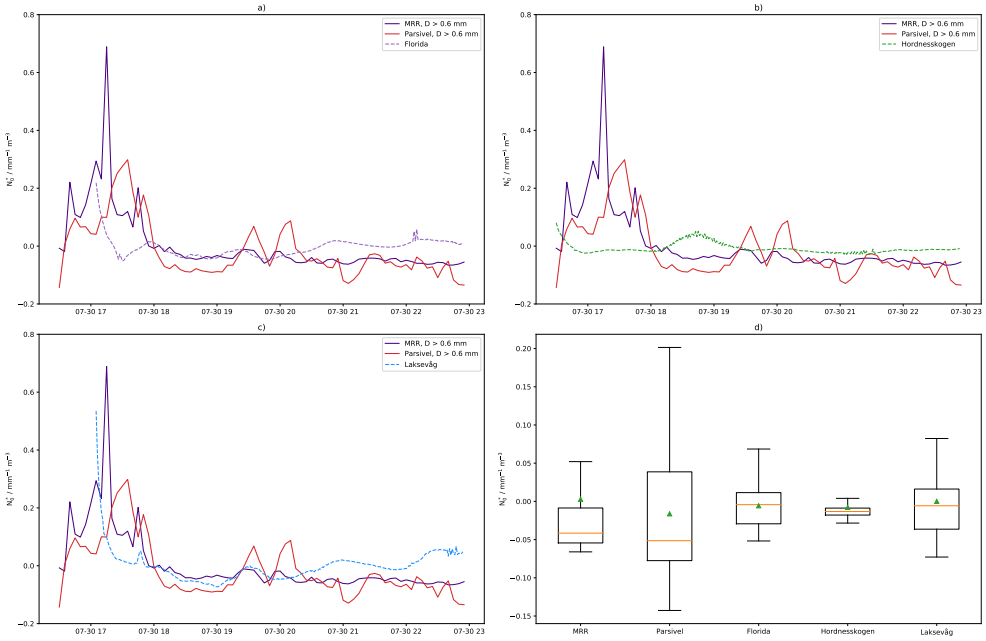

Figure 16: Same as for Figure 12 for the normalized intercept parameter (mm^{-1} m^{-3})

Overall, the model does a good job of predicting the calmer, stratiform period of precipitation. The sudden convective precipitation in the beginning is more uncertain in the model. Laksevåg captures this to some degree, but the start is delayed and has a slower increase. In addition the values does not quite reach the intensity measured in the observations. Here it is important to keep in mind the uncertainty of choosing a level for the precipitation start. The shape of the distribution is quite well represented in Hordnesskogen, but it is evolving much more rapidly and with much lower values. One also needs to keep in mind that different methods have been used for calculating the parameters for the model and the observations. This issue will be addressed in section 4

3.3 Vertical Characterization of the Precipitation Event

The microstructure of the rainfall has until now been characterized through three rainfall parameters, at one level in the atmosphere. In addition to this characterization it can be useful to examine the vertical behaviour of the precipitation in the atmosphere, for example to study droplet growth or other multi-layer processes.

I have therefore examined the vertical distribution of two parameters, the liquid water content (LWC) and the terminal fall velocity (V_T), to provide a more comprehensive understanding of precipitation events. The observed characterizations are presented first, followed by the model comparison. Observational data is presented for the MRR, as this is the only instrument providing vertical data. For the model representation, I have examined the same three grid points as for the one level comparison. Only Florida and Hordnesskogen will be presented in the following section, since they show two different aspects of the vertical model distribution. The result from Laksevåg was very similar to Florida, and is therefore not included.

Vertical Distribution of Liquid Water Content

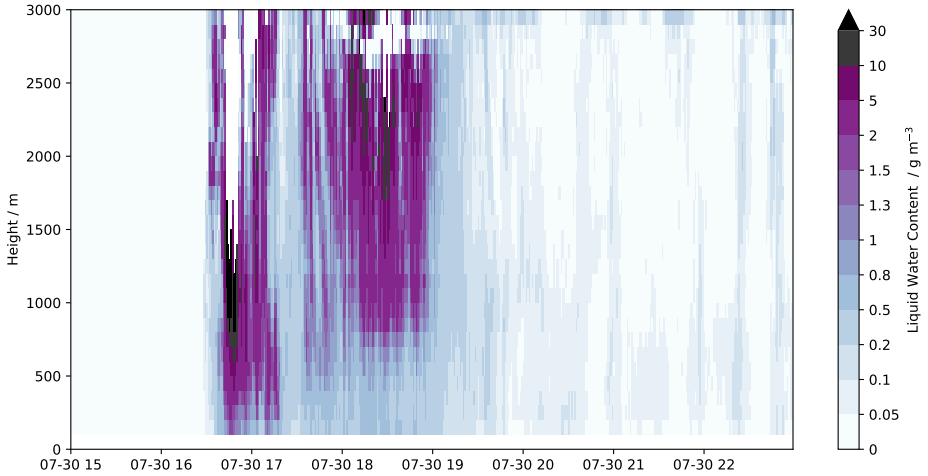

Figure 17: The distribution of observed LWC in the atmosphere at GFI on 30^{th} July 2019. LWC (g m^{-3}) is shown for the time 15:00-23:00, for the lower 3 km of the atmosphere, calculated from the MRR.

The vertical evolution of the LWC gives an overview of how the water was distributed in the atmosphere for the time of the event (Fig. 17). There are two periods of strongly enhanced LWC during the event. The first period marks the start of the precipitation (as seen from the rain rate in Figure 6), with the maximum values of LWC reaching up to 70 g m^{-3}. The core is located in the lower levels of the atmosphere, around 500-1700 m. The second period is located at a higher level, with a core around 2000 m. The values are weaker, reaching up to 20 g m^{-3}. Thus, the second period corresponds well with the weaker enhanced period visible from the rain rate (Figure 6). After 19:30, the LWC decreases below 0.5 g m^{-3}. The small LWC in the higher levels, mean the potential for droplet growtg is low. There are however, some fluctuations extending upwards in the whole column, indicating the presence of fall streaks. Aside from this the LWC is in general more stable below 0.2 g m^{-3}. This indicates a more stratiform type of precipitation compared to the beginning of the event. Note that there are two areas of no data (shown as white patches) in the period of high LWC, this is most likely due to attenuation. This means that the beginning of the event could have a stronger core higher up in the atmosphere that we can not see.

There are clear similarities between the observed LWC and the predicted LWC of Florida (Figure 18). The second period of enhanced LWC is also visible in the model. The core is located in the higher levels and appear at approximately the same time. The values however is much lower, with a maximum of 1.4 g m^{-3}, compared to the observed 20 g m^{-3}. The amount of water decrease after 20:00, with small fluctuations in LWC, similar to the observations. However, the fluctuations show more of a patch pattern compared to the observations, and several areas reach higher LWC values. There is for example an enhanced patch of LWC of 0.3 g m^{-3} extending horizontally in time around 1000 m height, indicating the presence of a stratus cloud in the model. The first enhanced period is missing entirely in the model, here there are only small patches of LWC around 500 m and 2500 m height.

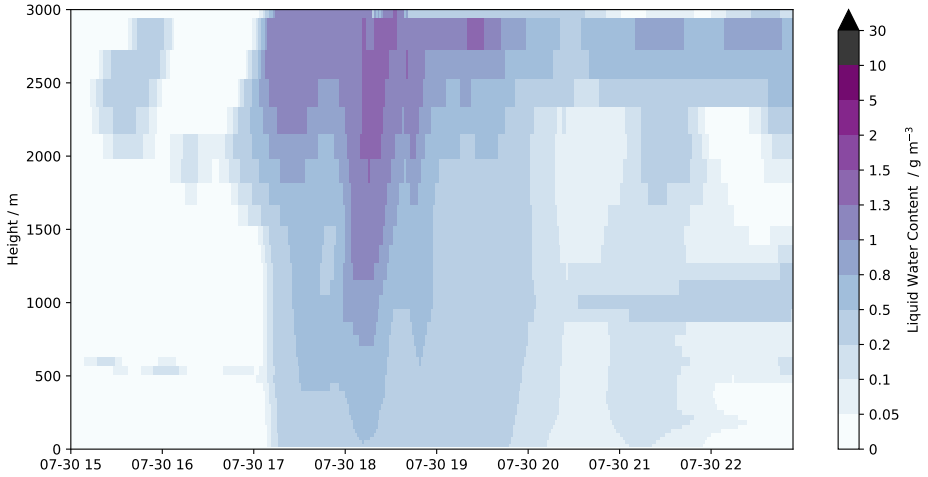

Figure 18: The distribution of predicted LWC in the atmosphere for 30^{th} July 2019. LWC (g m^{-3}) is shown for model point Florida for the time 15:00-23:00, for the lower 3 km of the atmosphere.

Hordnesskogen has a different distribution of LWC in the atmosphere compared to Florida (Figure 19). There are three distinct cores of enhanced LWC. The first corresponds well with the time of the first period in observations, however it is located at a higher level, with much lower values. This is similar to the differences found in rain rate (Figure 9). There is in addition some LWC present before 16:00, at higher levels for Hordnesskogen, which is not the case for the observations. The second core is in the same time range as the second observed peak, but it occurs earlier and is located at a lower level. The shape is in addition much narrower, supporting the compressed evolution of rain rate (Figure 9). The third core occurs between 19:00-20:00, in the higher levels of the atmosphere. This is not present in the observations. There are variations in LWC after this period, but more patches than fluctuations. The LWC after 19:00 has higher values extending further down in the atmosphere compared to the observations. There are several areas of LWC around 0.5 g m^{-3} above 1000 m. In summary, both model points capture part of the event by placement of the core, however the values are much lower compared to the model and Florida is completely missing the first enhanced LWC.

The Terminal Fall Velocity

The vertical distribution of the observed terminal fall velocity of the drops show rapid variations throughout the precipitation event (Figure 20). Linking the velocity to drop sizes, this indicates a spectra of different drop sizes during the precipitation. The maximum velocity is measured to 9.5 m s^{-1}, which according to the relation of Foote and Du Toit (Foote and Du Toit, 1969) would imply large drops up to 6 mm. These size was not seen in the lower level from the study of the DSD (Figure 10). The largest size with the concentration cutoff in place was measured to be 3.06 mm. Without this cutoff, drops up to 5 mm were measured with a mean number concentration of 10^{-2} mm^{-1} m^{-3}. The maximum strength occurred several times, corresponding well with an increase in rain rate for the same time periods (Figure 6). There are three short periods of strong velocity extending over the whole vertical column, in the time around 21:00, 22:00 and 23:00, indicating the presence of fall streaks in the atmosphere. A longer time period

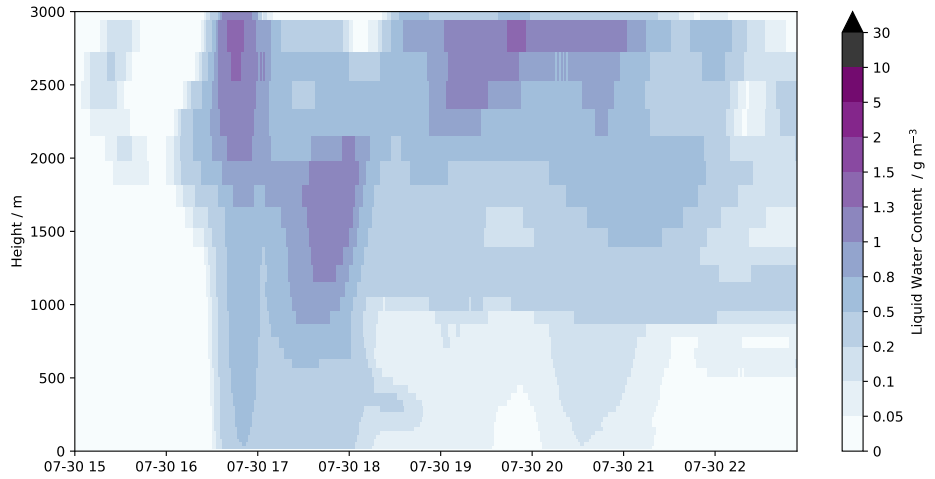

Figure 19: Same as for Figure 18 for model point Hordnesskogen.

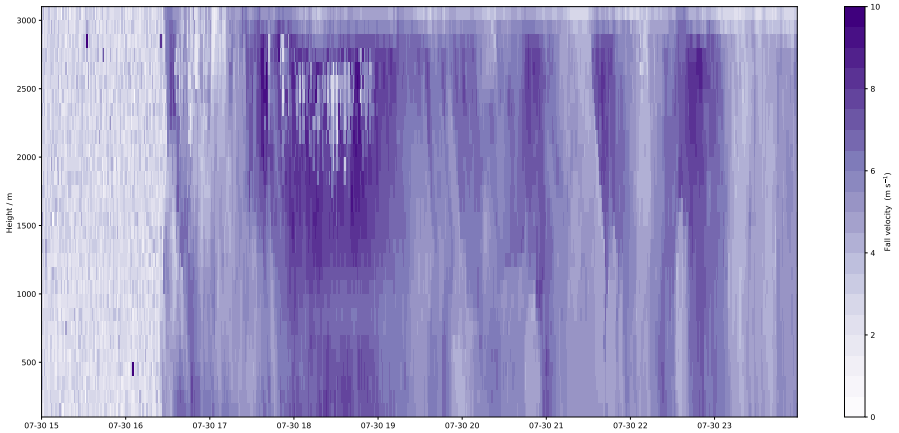

Figure 20: Vertical distribution of the observed terminal fall velocity V_T (m s^{-1}) for the lower 3 km of the atmosphere. Showing the evolution for the precipitation event in at GFI from 15:00-23:00 UTC on 30^{th} July 2019.

of enhanced velocity is present between 18.00-19.00 for the whole atmospheric column. This indicates a dominance of larger drop sizes for this period. The investigation of full drop size spectra versus the limited drop size spectra for LWC (Figure 11) also proved this to be the case. This period in time did not experience significant changes when excluding the small drop diameters. The highest intensity period of rainfall show weaker fall velocity compered to the second enhanced period, again implying that the first period was dominated by smaller drops. The mean terminal fall velocity of the entire precipitation period was 5.3 m s^{-1} (which has been used to determine the starting level for precipitation in the model, Figure 9). Note the area of missing data in this period between 2000-2500 m, most likely due to attenuation, as seen from the LWC (Figure 17).

The predicted terminal fall velocity of point Florida (Figure 21) shows coarser structured pattern compared to the observations. Nevertheless, there are several similarities. The three periods of maximum velocity around 5 m s^{-1} occur around the same

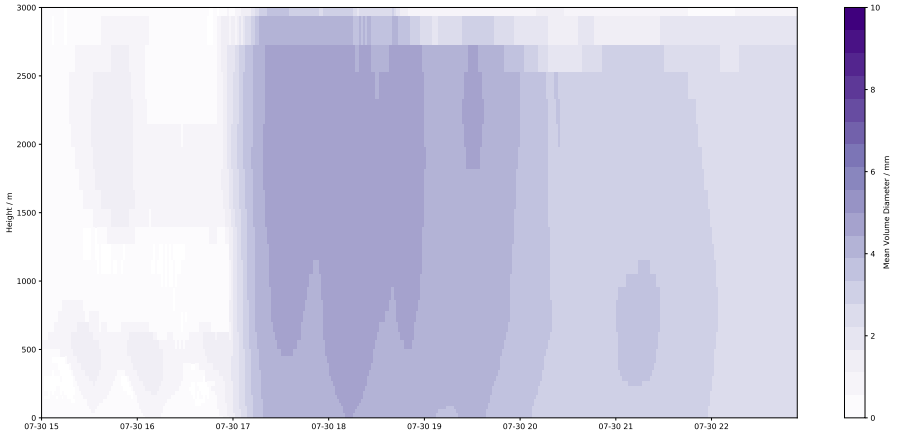

Figure 21: Vertical distribution of the predicted terminal fall velocity for the lower 3 km of the atmosphere (m s^{-1}). Showing the evolution for the precipitation event in model point Florida, from 15:00-23:00 UTC.

time as observed maximum period (only weakened in strength). The times are again corresponding with increasing rain rate (Figure 9). This is not unexpected, as the calculations for the fall velocity is dependent on the specific content of rain water in the atmosphere (see section 2.4). However the observations also have three maximum periods at the higher levels after 20:00, which are not present in the model point. The observations also show a lower level increase in velocity around 21:00, this is clearly captured by the model. There are less variations in velocity after 20.00, we have a more uniform distribution throughout the atmosphere. The calculations are based on a relation between drop diameter and mass. We know from the study of rain rate (Figure 9) that also the precipitation was more uniform in the model compared to the MRR. The weaker velocities in the model indicate a prediction of smaller drops in the model compared to the observed drop sizes. Velocity up to 5 m s^{-1} would correspond to a drop of approximately diameter 1.5 mm, which is only half the size of the observed maximum drops. The lower drop size was visible in the comparison of mean volume diameter (Figure 14). Keep in mind for further discussion (section 4) that the model only calculates mean volume diameter, while the instruments can display all drop sizes.

Point Hordnesskogen on the other hand only show one period of maximal velocity (5 m s^{-1}), around 19:00 (Figure 22). The velocity decreases after this, but there are several periods of enhanced fall velocity, again corresponding to small increases in precipitation (Figure 9). These pattern roughly match increased V_T in the observations as well. However, the strongest period in the observations between 18:00-19:00 is not visible in Hordnesskogen, as precipitation decrease at that time (Figure 9).

The calculation of mean volume diameter and terminal fall velocity for the model is related to each other, and based on several assumptions which contributes to uncertainty. The implications of these uncertainties will be further addressed in the discussion, section 4

To get a better overview of the thermodynamic situation in the model during the event, a representation of the equivalent potential temperature and all the precipitating components are included (Figure 23). The equivalent potential temperature can provide information on the stability in the atmosphere. During the precipitation period, a slight

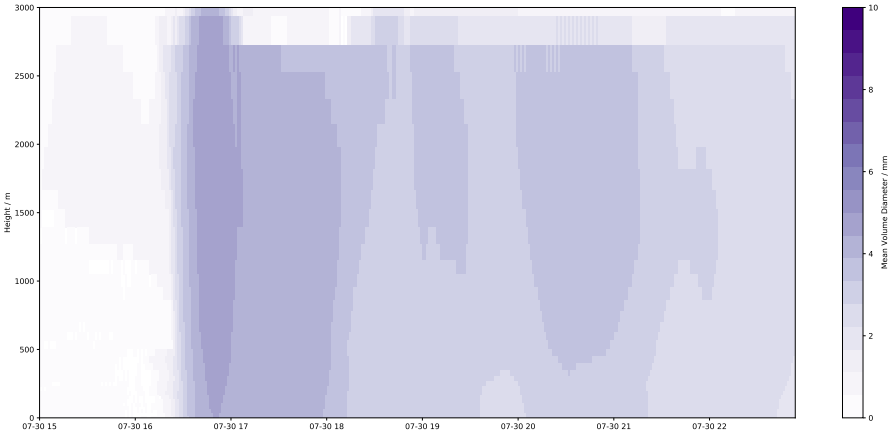

Figure 22: Vertical distribution of the predicted terminal fall velocity for point Hordnesskogen during the precipitation event, (m s^{-1}.

increase in temperature can be seen throughout the atmospheric column. There is negative vertical velocity, which means we have updraft in the model. All the precipitating species are present in the higher levels. Again, we can see that the model does not predict anything before 17:00, and the strongest values occur around 18:00. The lower levels are dominated by rain water and liquid cloud water. Around the melting level, situated around 3200 m, we see some gathering of snow and graupel. Ice is present in the higher level, but only occur later in the evening, around 19:00. The distribution of these precipitating species is very similar to the LWC (Figure 18), as we would expect. We do not have available these characteristics for the observations and can therefore not conduct a comparison on this. Still, it provides a good overview for the model situation and was therefore included in the study.

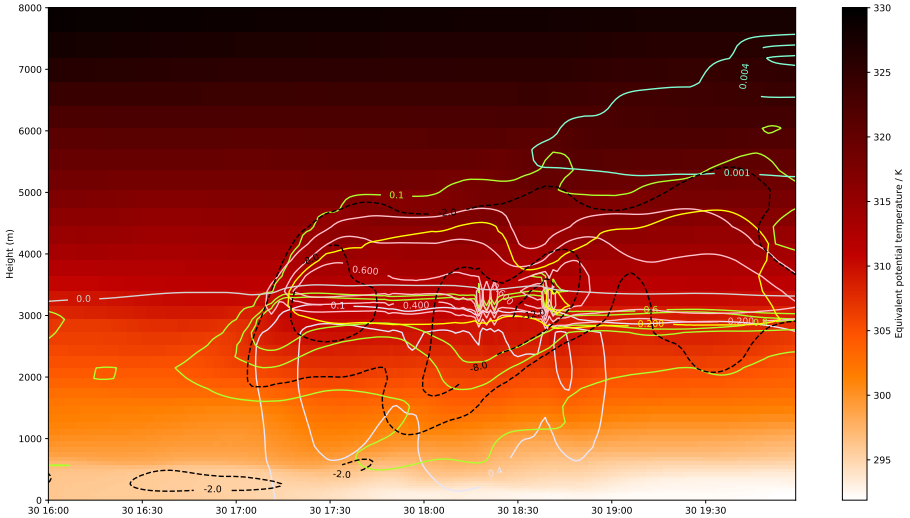

Figure 23: Predicted equivalent potential temperature (shadings, K) with the distribution of the different predicted water species components for the time period 16:00-20:00 UTC, for Florida. The specific content of rain water (lavender), cloud water (green), ice (aquamarine), snow (pink), graupel (yellow) (g kg^{-1}). The vertical velocity (m s^{-1}) is shown in black and the zero temperature line in grey.

The situation for Hordnesskogen looks quite different in terms of distribution (Figure 24). Here most of the activity occur between 16:30-17:00. There is still activity later, but it is weaker. There is one patch of cloud ice present in the higher levels between 17:30-18:30.

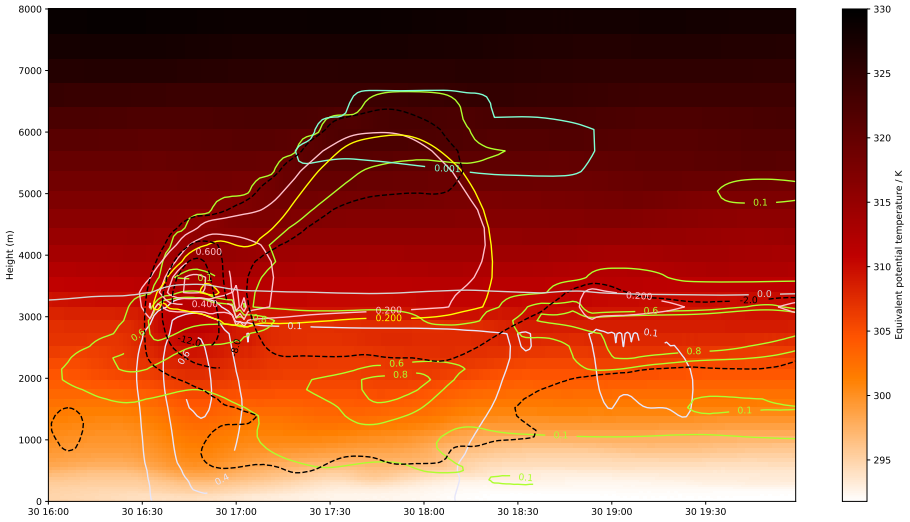

Figure 24: Same as Figure 23, but for Hordnesskogen

3.4 A Sensitivity Experiment for Parameter tuning in the Model

The intercept parameter, N_0, has a large impact in several aspects of the model calculations. For example, AROME-MetCoOp base the calculations of the water species on the assumption that N_0 is the constant from the Marshall-Palmer distribution (Seity et al., 2011). From the study of the observed DSD, we could see that the precipitation roughly followed the Marshall-Palmer distribution. However, there was a change for the different drop sizes and the two different instruments showed opposite signs.

This allows me to conduct a small sensitivity experiment regarding the plausible range of values of N_0. The rainfall variables where it is possible to adjust this intercept parameter, for this thesis, is the mean volume diameter (D_m) and the terminal fall velocity (V_T). I have performed a sensitivity experiment using different values for the intercept parameter (N_0). Oservations for different types of rain show a range of values for the intercept parameter (N_0) from $0.4 \cdot 10^7$ to $3.5 \cdot 10^7$ m^{-4} (Méteo-France, 2009) . The Marshall-Palmer constant is $8 \cdot 10^6$ m^{-4}. For this study and the comparison I have used the model points Florida and Hordnesskogen, which are then compared to the observations.

Plausible range of the intercept parameter in calculations for the mean volume diameter

The mean volume diameter shows large variations in size by changing the values of the intercept parameter N_0 (Figure 25). The larger the values for N_0, the smaller the diameter becomes. Florida was already quite well within the range of the observations based on the original calculations, using the Marshall-Palmer constant (Figure 25 a). However, an interesting observation here is how many of the values for N_0 match the range of the observations. The only line never matching the observations is the one

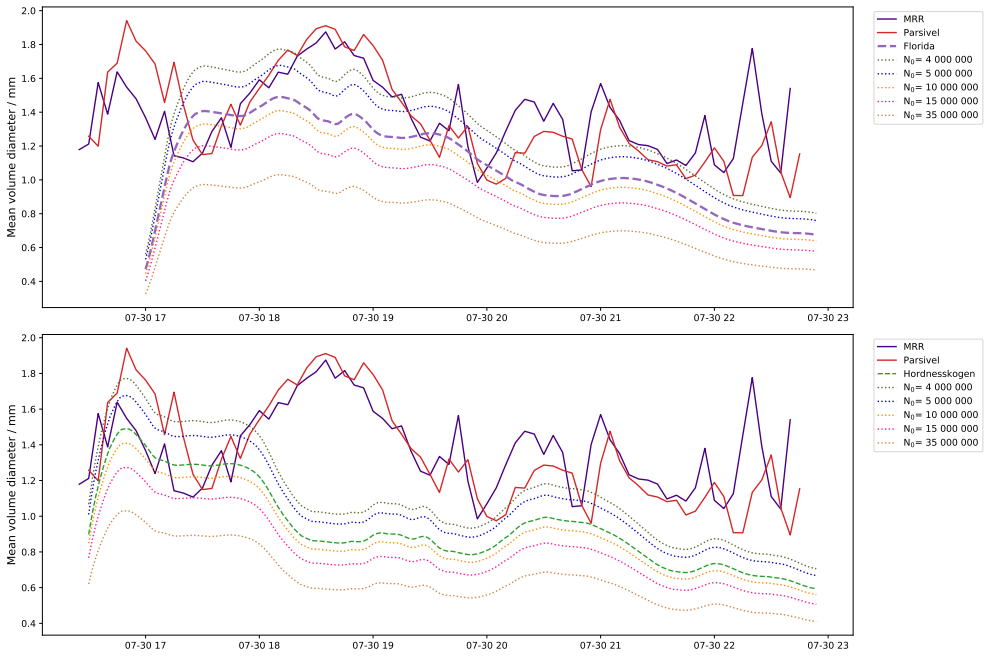

Figure 25: The mean volume diameter (mm) for the time period 16:30-23:00. Observed mean volume diameter for the MRR (indigo line) and the Parsivel (red line). Compared to the mean volume diameter of the model for different values of the intercept parameter N_0 (dotted lines). a) Model point Florida (the purple dashed line is the constant Marshall-Palmer N_0). b) Model point Hordnesskogen (the green dashed line is the constant Marshall-Palmer N_0).

for the largest intercept parameter ($N_0 = 3.5 \cdot 10^7$ m^{-4}, brown line). All the others are within the observed size range. Already here, we see that determining a value for the intercept parameter is challenging. Both $N_0 = 0.4 \cdot 10^7$ m^{-4}, (olive line) and $N_0 = 0.5 \cdot 10^7$ m^{-4} (blue line) corresponds better to the observations in terms of the values for maximum and minimum diameter. The maximum is close in value, just shifted a bit in time. However, for some of the fluctuations in the observed values these show a diameter much larger than the observed diameter. For these points, the Marshall-Palmer constant (purple dashed line) and $N_0 = 1 \cdot 10^7$ m^{-4} (orange line) are closer. The shape of the evolution is not affected, since we keep to constant values for the intercept parameter (N_0).

The mean volume diameter for Hordnesskogen (Figure 25 b)), when using the Marshall-Palmer constant N_0, match well with the observations in the first 1.5 hours. After this the diameter is smaller for the model. For the other values of N_0, we see that both $N_0 = 1.5 \cdot 10^7$ m^{-4} (pink line) and $N_0 = 3.5 \cdot 10^7$ m^{-4} (brown line) is smaller than the observed diameter. The smallest intercept parameters match better with the overall evolution of the diameter. Yet, it is much smaller than the observations for most times after 18:00.

Plausible range for the intercept parameter in calculations for the terminal fall velocity

The terminal fall velocity is also clearly impacted by the change in the intercept pa-

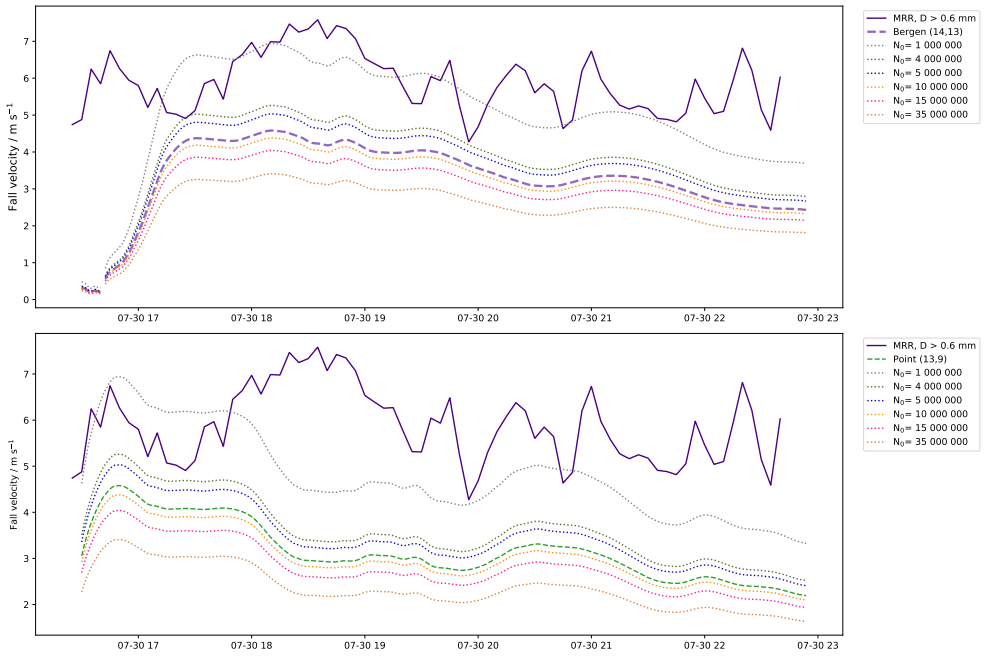

Figure 26: The terminal fall velocity (m s^{-1}) for the time period 16:30-23:00. Observed terminal fall velocity for the MRR (indigo line) compared to the predicted, for different values of the intercept parameter N_0. The comparison is performed at the height of MRR (345 m a.s.l). a) Model point Florida (the purple dashed line is the constant Marshall-Palmer N_0) b) Model point Hordnesskogen (the green dashed line is the constant Marshall-Palmer N_0).

rameter (N_0) (Figure 26). Again, we see a decrease in the rainfall parameter when the intercept parameter increases. Both Florida (Figure 25 a) and Hordnesskogen (Figure 25 b) had vertical velocity lower than the observations. Thus, here we see that even the smallest N_0 within the range of observed values barely reach the minimum values of velocity for Florida, and not at all for Hordnesskogen. I added an extra $N_0 = 0.1 \cdot 10^7$ m^{-4} (grey line) to see how much smaller the intercept parameter had to be to give diameters in the range of the observations. Florida now lies quite well within the observations, with a maximum speed only about 1 m s^{-1} smaller. The are some fluctuations present, but they are fewer and more elongated. Hordnesskogen now gets too high values at the beginning of the event, but other than that the values are mostly still below the observations.

The two rainfall parameters investigated are related in the calculations used in this study. There are also quite a few assumptions made to make the calculations possible. All this results in a higher uncertainty for the experiment. Still, the study provide a quick-look into how important these parameters are in the model. And it becomes clear how difficult it can be to select a single value for N_0. I will further discuss the topic in section ....

4 Discussion

In this section I will do an evaluation of the approach I have derived throughout the thesis. I will examine how well the overall approach performed, and give an overview of the advantages, limitations and uncertainties to the methodology. Then I will discuss the value of high-resolution comparison as opposed to longer time-resolution, and see if the same results could be accomplished with an hourly time resolution.

4.1 Measurement Uncertainty

Four different instruments providing measurements of precipitation characteristics have been investigated in this study. When using instruments with different measuring methods some variations are to be expected, as each instrument comes with its own accuracy and uncertainty. In this section, I will evaluate the impact of the variability for the four instruments during the precipitation event on 30^{th} July 2019.

From the examination of rain rate (Figure 6), it became clear that the overall evolution of the precipitation event was captured in a similar way for all instruments. The high-intensity period however, showed relatively large differences in time and intensity. The MRR had the highest intensity in rain rate, in addition the whole evolution was shifted 5 minutes earlier than the others (except for the TPS who proved to have a 5 minute later time shift). The MRR measures at a height level of 300 m above the Parsivel and the TPS, and 345 m above the AWS. This provides a likely explanation for the earlier shift in time, and at least partly for the higher intensity.

The Parsivel measured the lowest intensity during the high-intensity period. The struggle to realistically capture heavy rainfall is a known problem for the Parsivel (Wen et al., 2017). It is prone to underestimation of the rain rate in these situations.

I make a limited study of the correlation between rain rate and wind speed and direction for the summer months for each instrument, with the AWS as the reference (figures not shown). This was done to examine if wind conditions during this period of time had a tendency to affect the instruments in regards to precipitation measurements. I wanted to test if different exposure to wind could be responsible for some of the variations in rain rate. However, the summer months of 2019 proved in general to have low wind speeds (below 4 m s^{-1}) and there was no measurable correlation between the rain rate and the wind speed.

Further characterization of the precipitation in this thesis is done through the weighted moments of the DSD, from the MRR and the Parsivel. Since these where the two instruments most variable in rain rate intensity a thorough investigation of the number concentration with respect to drop diameter was performed for both instruments. Despite the difference in rain intensity and the difference in measurement height, proved the MRR and the Parsivel to be quite consistent during the event. This was especially the case when excluding the smallest and largest drop sizes, which have proven to have higher measurement uncertainty for both the MRR and the Parsivel (Wen et al., 2017).

4.2 Uncertainty in the Derived Methodology

The main goal for this thesis was to derive a new methodology that enabled a direct comparison between high-resolution observations and time-step output of the operational NWP model. In this section I will discuss some of the uncertainties and limitations of this approach.

All observational rainfall parameters are calculated through the weighted moments of the DSD. The uncertainty associated with this aspect have already been comprehensively studied in the results in section 3.2.2.

The same rainfall parameters have been calculated for different model grid points. However, the model provides different variables than the instruments. Therefore, the predicted rainfall parameters had to be obtained through a different methodology compared to the observations. This, of course introduces an added level of uncertainty.

The first challenge was encountered when deriving the rain rate. The model output does not directly provide rain rate. Instead, the specific rain water is available for the whole atmospheric column. Not all of this water will fall as precipitation. We therefore had to decide on a starting level for precipitation in the model. I chose to use the relation of speed, time and distance for deciding on this starting level. I based this on the mean observed terminal fall velocity from the MRR. The starting level obviously has an impact on the amount of precipitation predicted from the model. With this approach we know that there is a sensitivity of the intensity of precipitation and thus the accumulated precipitation using the terminal fall velocity. The mean V_T could vary based on how the time of the event is defined. In addition, the V_T of the model was proven to be weaker than the one observed, this would have given a lower level for the starting point of precipitation.

Two of our model points, Hordnesskogen and Laksevåg, would have benefited from a higher starting level for precipitation providing a higher intensity for the rain rate. This would have given us a maximum intensity in point Hordnesskogen and Laksevåg, that would have come closer to the observed intensity. However, the model point Florida would have ended up with a poorer correspondence to observed rain rate.

In addition, the evolution of rain rate would not have changed by changing the intensity. Neither Hordnesskogen or Laksevåg had a "perfect" match in evolution, developing to fast and to slow, respectively. Except for the missing high-intensity precipitation in the beginning, Florida on the other hand, had a very good fit for the rest of the event. The absence of an apparent systematic bias provides confidence that we can move forward with this approach for choosing the level of precipitation, while keeping in mind the uncertainty.

Another aspect of uncertainty is introduced during the calculation of LWC. The model predicted LWC is based on a summation of rain water and liquid cloud water. This is multiplied by the model density.

The model output extracted by the combined use of AROME-MetCoOp and DDH does not provide density. The density was therefore calculated from the equation for hydrostatic balance. We assume this to be a close enough approximation, since density is expected to only have small changes over smaller areas. Still, this is yet another point

of uncertainty for the model calculations.

The LWC examined in one level for Florida missed the high-intensity precipitation, as no rain or liquid cloud water was present in the model for this time. Convective precipitation is proven again to be a challenge for the model. However, the more stratiform period of precipitation was very well predicted (Figure 12). Hordnesskogen showed an underprediction of LWC throughout the whole time period, while Laksevåg had two periods of overprediction, otherwise it was mostly realistically predicted. This corresponds very well to the findings of Conrick and Mass (2019). Their model overall proved adequate prediction of LWC compared to the observations. Then they dived the precipitation prediction into three categories: underpredicted, realistically predicted and overpredicted. The LWC was found to corresponded to the prediction categories for the precipitation. This is the same results as what we observe in the different model grid points for AROME-MetCoOp.

The vertical distribution of LWC in the atmosphere shows more differences compared to the one level comparison. The maximum values provided in the model was greatly underestimated compared to the observations. We keep in mind here that the model provides average values for the whole column between two model levels, which therefore does not include maximum values in the same way the observations does. Smoother characterizations and some lower values are to be expected. However, there is quite some uncertainty to how much difference can be explained by this fact.

Several assumptions are made for the calculations of the mean volume diameter and the terminal vertical fall velocity. The mean volume diameter is calculated based on a relation with the terminal fall velocity and mass. In the terminal fall velocity calculations, uncertainties regarding the use of the constant Marshall-Palmer intercept parameter and a gamma distribution are introduced. The influence of other values of the intercept parameter was examined in the sensitivity experiment in section 3.4 and will be discussed in the following section 4.

The mean volume diameter was mostly prone to underestimation in the model. This differ from Conrick and Mass (2019) who found their measurement of drop size to be substantially larger than the observed drop size. However they used the median volume diameter as opposed to the mean volume diameter used in this study. It is therefore hard to compare the results here.

The calculated normalized intercept parameter however was modestly underestimated in Conrick and Mass (2019). We found the parameter to be within the range of the observations, only with a narrower range of values.

4.3 Sensitivity to Parameters in the Model

The comparison of high-resolution observations and model output brought forth another aspect of NWP models that is worth investigating further. Several assumptions and constant parameters are taken in use in the model calculations. This is unavoidable. However, the comparison on higher resolution made the importance of these constant parameters very apparent. Additional parameterisation of these parameters will become even more important in the future, as more studies shift focus to higher time- and spatial-resolution. For example the study of Valkonen et al. (2020) as mentioned in the introduction.

As an example for investigating the importance of one of these parameters, I used the number concentration intercept parameter and conducted a limited sensitivity experiment (section 3.4)

The intercept parameter is constantly up for discussion, as choosing a value for the models remains problematic (Thompson et al., 2008). This was also the result in the sensitivity experiment. Several of the values for N_0 gave acceptable results for the mean volume diameter (Figure 25). However, none of the original values within the usual observed range proved sufficient to increase the vertical velocity.

The challenge here may lie in the limitations of using a constant value for the intercept parameter. The drizzle droplets are limited from interaction with other precipitation species, due to the direct transfer from cloud water to rain in the model (Thompson et al., 2004). This could be one of the reasons the model provide smaller drop sizes compared to the observed diameters. The parameter has often been observed not to be of constant value, for example, the value for N_0 is much larger for warm-rain (drizzle) processes compared to the process for melting snow (Engdahl et al., 2020). A possible alternative approach could be to make the number concentration N_0, a stochastic parameter in the model.

4.4 Investigating the Value of High-Resolution Comparison

I have based this thesis on the hypothesis that higher time-resolution would benefit the characterization of precipitation and the comparison between model output and observations. I argued that a high-resolution comparison would give a clearer understanding of where the model captures the observed situation and where it faces challenges.

Throughout the thesis, I have presented a detailed comparison between the observed characteristics of the precipitation event and the predicted event from the combined DDH and AROME-MetCoOp model extracted output. Now I will investigate closer on whether this high-resolution comparison actually provides more knowledge on the precipitation event. I will compare the high-resolution results and against hourly data.

I have chosen the most used parameter for precipitation, the rain rate, to investigate the difference in resolution (Figure 27). Thus, a comparison is performed on the high-resolution rain rate (mm $5min^{-1}$, Figure 27 a) and the hourly accumulated rain rate (mm h^{-1}, Figure 27 b).

At first glance the evolution of the hourly rain rate look very similar to the high-resolution data. Precipitation starts later in the model point Florida compared to the observations. The maximum intensity is still lower than the observational mean and located in the same time interval.

The more uniformly distributed rain rates of Florida and Laksevåg keep the maximum intensity in the right time interval. Laksevåg however now has the overall maximum intensity. This was not the case in the high-resolution result. There, we could see that the rain rate was distributed more uniformly over the hour interval, compared to the observations that had a large peak at the end of the hour.

The more skewed evolution of Hordnesskogen and the observational mean gets a shift

in maximum to the hour later (Figure 27, green line). For these two points, especially for Hordnesskogen, the maximum intensity of rain expected in this period is seen as greatly reduced. The amount is of course still the same, but now it is evenly distributed throughout the whole hour interval. This was not the case for the higher resolution, where the same amount occurred in the last 20 minutes of the hour. Here we see a clear example for how the higher resolution provides more detailed information. Some fields, for example agriculture, greatly benefit from a detailed knowledge about the intensity of the rain rate. The same amount of precipitation can make a big difference. Evenly distributed precipitation is good for the soil, however to much water rapidly can cause great damage. The same concept applies for landslides and flooding, it is most often the intensity over a short time period that cause the most damage. To be able to pinpoint the location and intensity of the precipitation is therefore very useful in cases like these.

Overall, the hourly data provides us with a lot of the same information. We see a similar evolution, we see variability in the model grid points and we see similarities and differences in model compared to observations. However, the higher time resolution give a much more detailed look into intensity and timing, which is smoothed out for the hourly data. From this it is clear that the model struggles with the high-intensity precipitation and the rapid start of the rainfall. The convective start of the precipitation is not as clear in the hourly interval, and we would maybe not have thought to look for the feature in other model grid points had we only examined the hourly data.

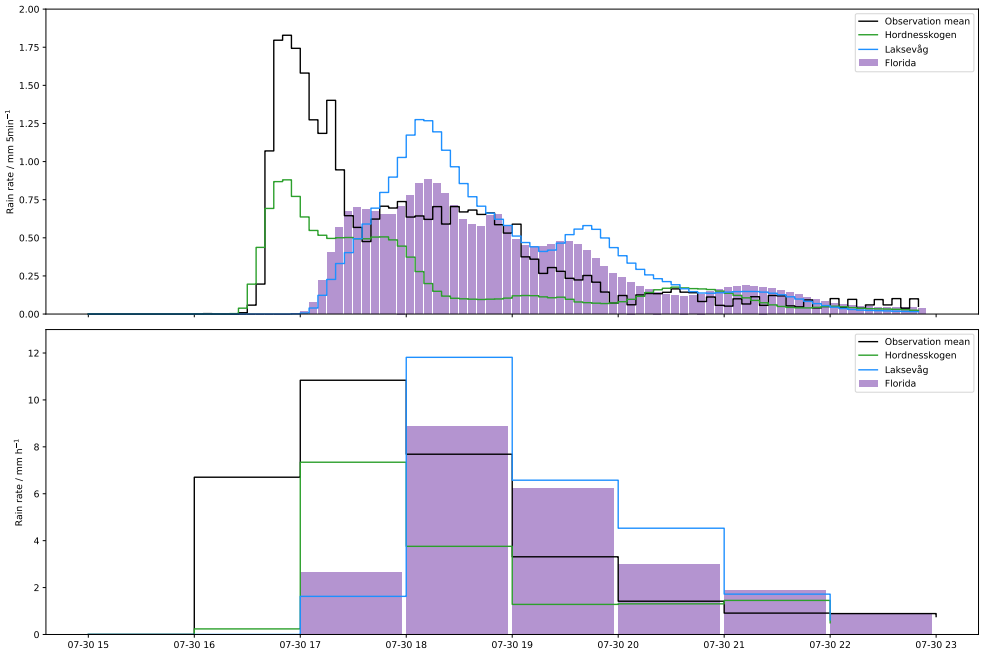

Figure 27: Comparison of rain rate for a) high-resolution time intervals of 5 minutes mm 5min^{-1} and b) hourly time intervals mm h^{-1}. Included are the observed mean (black line) and the model grid points: Florida (purple bars), Hordnesskogen (green line) and Laksevåg (blue line), for the time period between 15:00-23:00 UTC.

5 Summary

The goal of this thesis was to enable a direct comparison between high-resolution precipitation observations and the operational weather prediction model output. Extensive work was put into deriving a methodology making this comparison possible. An example of the use of this methodology was presented through a high-intensity precipitation event occurring in Bergen on July 30^{th} 2019.

To conclude this work, I will discuss the main findings in relation to my key research questions:

1. How can we characterize the precipitation in a way that make it possible to compare high-resolution observations and model data?

We extracted a detailed prediction of the diagnostic parameters in the model for every model time step over a chosen subdomain, centered around the point of observations. A time-resolution of 5 minutes was used for both observations and model output. Five different rainfall parameters have been the key focus in this study: rain rate, liquid water content LWC, the mean volume diameter D_m, the normalized intercept parameter N_0^* and the terminal fall velocity V_T. All of these parameters could be presented for both model and observations. Then, two different aspects of the precipitation event were investigated. The first was a comprehensive characterization of precipitation on the model and instrument ground level, using rain rate, LWC, D_m and N_0^*. Second, a vertical distribution of LWC and V_T provided a characterization of the behaviour of the precipitation event upwards in the atmosphere. Together, they gave an overview of how the liquid water was distributed and at what fall velocity the droplets moved towards the ground, thereby also giving an indication of the drop sizes present in both observations and model.

2. How does AROME-MetCoOp perform compared to high-resolution observations of precipitation?

An evaluation of the performance of the model prediction were executed using a closest point approach. Six different points of interest was examined in comparison with the observations by means of the rain rate. From this, three points were chosen for further characterization. All points featured different aspects of the precipitation characteristics present in the observations. All three points had individual features of similarities with the observed precipitation event, in terms of start of precipitation (Hordnesskogen), intensity (Laksevåg) and evolution in time (Bergen). However, everyone of them also showed features of large deficiencies to the observations. In terms of weaker intensity (Hordnesskogen), a missed peak and delayed start (Florida), and unfitting evolution (Laksevåg). Thus, we can conclude that AROME-MetCoOp captured aspects of the precipitation very well. Especially the stratiform period during the evening had a generally good correspondence to the observations. However, some aspects of the precipitation are clearly still a challenge for the model. For this event, the model especially struggled with the high-intensity start of the precipitation. Laksevåg showed a similar peak feature, but it had a slower start compared to the observations and was quite delayed. The vertical comparison of LWC and V_T showed some of the same challenges. The model struggled to capture the maximum of the observations. Both LWC and V_T was clearly underestimated for the highest intensity period. This also indicates an underestimation of the drop size in the model.

Overall the high-resolution comparison provided a very detailed knowledge about similarities and differences between model and observations. The importance of location in the model was made very clear. Because even though the high intensity feature was visible in some of the grid points it was completely missed in most of them, as was the case for the prediction for Florida.

In this thesis I have made a substantial effort to derive a methodology needed for enabling this type of comparison between high-resolution precipitation observations and the operational weather prediction model output. I have also provided an example for how this methodology can be of use. However, this is only one precipitation event, it would therefore be interesting for further work to explore more of these types of events for more extensive knowledge about the precipitation characteristics and how the model capture it. Especially, it would be of interest to see if some of the same similarities and challenges are visible in similar events. In addition, I have focused on high-intensity precipitation in this study, but the methodology can be applied to all types of precipitation events. A further examination of other types of precipitation would also be interesting. For example, snow behaves quite differently to rainfall and may exhibit a different type of DSD (Engdahl et al., 2020). An investigation into how this would affect the characterization and thus the comparison could be very intriguing.

6 Appendix A

6.1 Rain rate

A complementary figure for the comparison of observed 5 minute rain rate with six different model grid points from section.... This provides a closer look on each chosen grid point for the comparison of rain rate with observations (Figure 28).

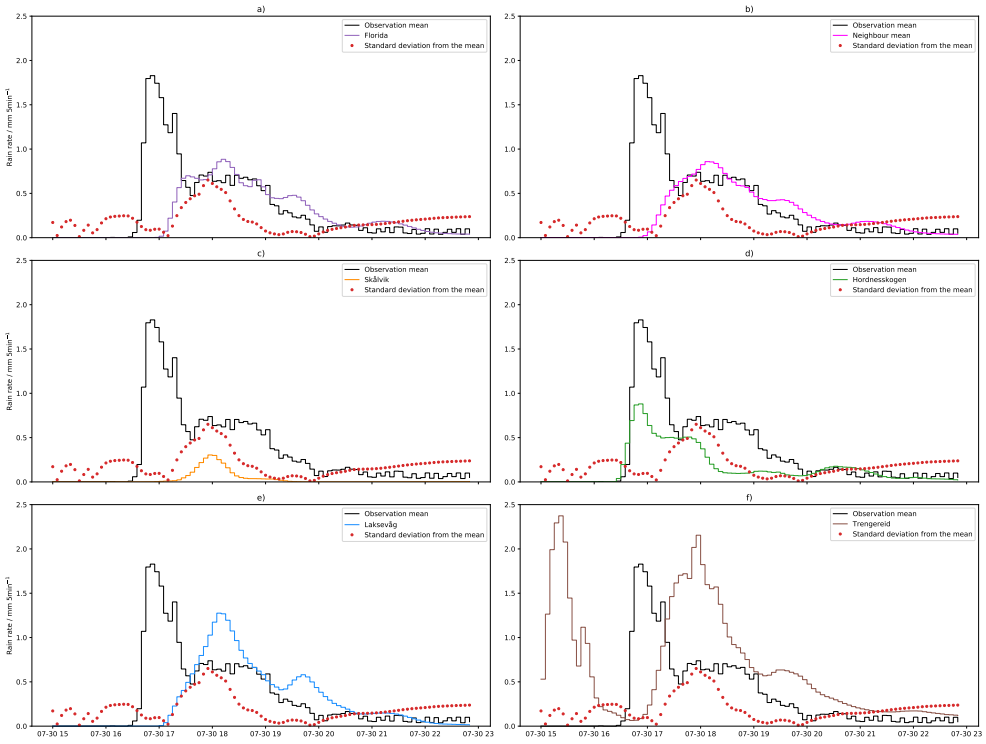

Figure 28: A comparison of observed and predicted accumulated 5 minutes rain rate (mm 5min^{-1}). The observational mean of the instruments (black line) is compared to a) the grid point representing instrument location, Florida (purple line). b) the mean of all neighbour points with Bergen as center (magenta line) c) Skålvik (orange line), d) Hordnesskogen (green line) e) Laksevåg (blue line) and f) Trengereid (brown line). The standard deviation from the mean is shown in red

6.2 Hourly mean drop size distribution

A complementary figure to the investigation of drop size spectra in section ... Presented here is the mean number concentration for every hour during the precipitation time in the instruments. There are variations in the instruments, but we again see that this is mostly the case for the smallest drop sizes. The high intensity period of rainfall show to in relatively good agreement with the higher Marshall-Palmer reference lines. While from 20:00 and on wards the weakest rain rate proves the best fit.

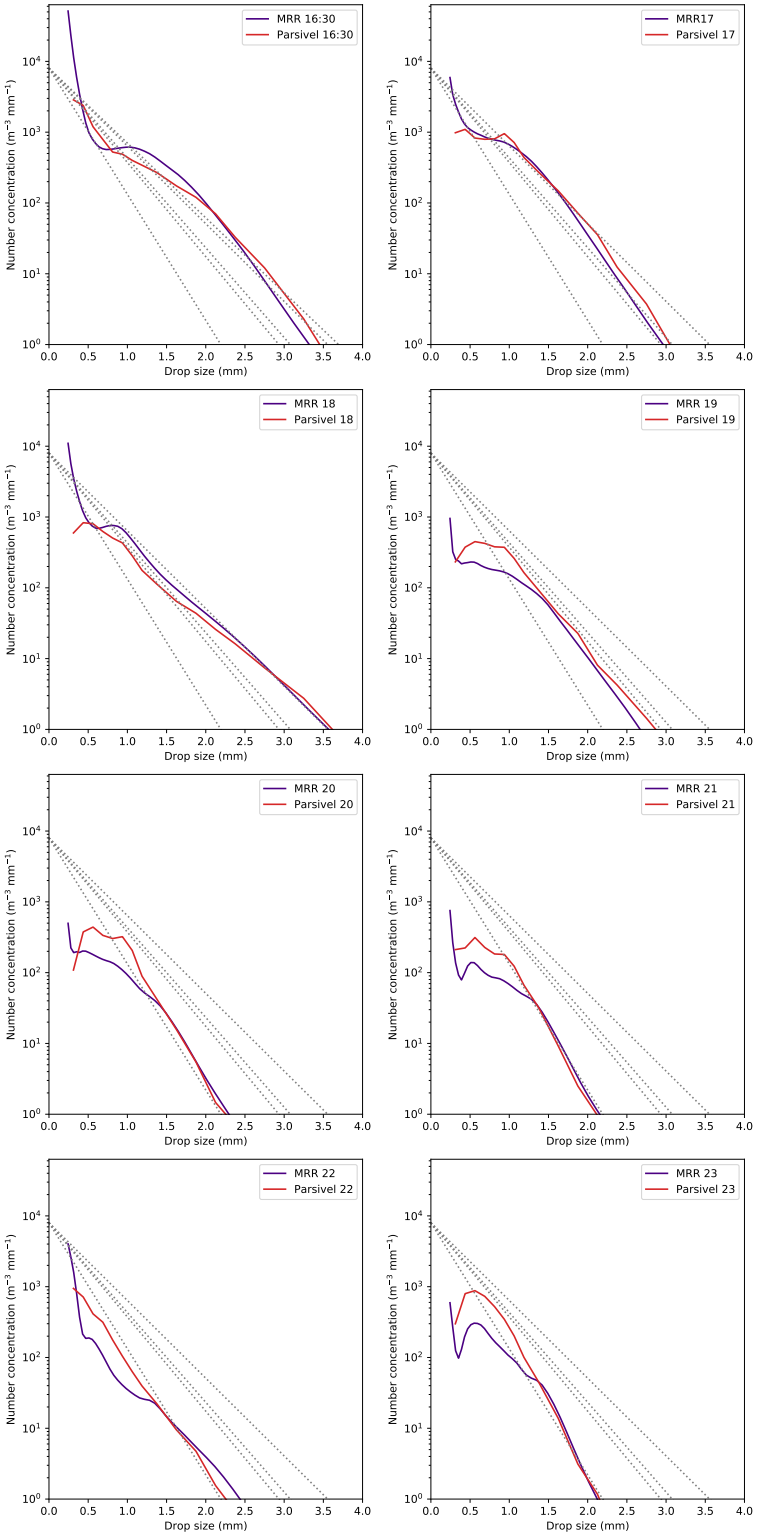

Figure 29: The mean number concentration (mm^{-1} m^{-3}) with respect to drop size (mm) for each hour. A comparison between the MRR (indigo line) and the Parsivel (red line) a) 16:30-16:59 UTC (from the starting point of precipitation), b) 17:00-17:59 UTC c) 18:00-18:59 UTC d) 19:00-19:59 UTC e) 20:00-20:59 f) 21:00-21:59 g) 22:00-22:59. Marshall-Palmer reference lines are presented for rain rate 1 h^{-1}, 4 mm h^{-1}, 5 mm h^{-1}, and 10 mm h^{-1} (grey dotted line)

6.3 Vertical LWC and V_T for Florida

The investigation of the vertical distribution for the LWC, and V_T for model point Laksevåg. The strongest core from Florida (Figure 18) is not present here, and there are small patches of variations in the lower level. Apart from this the point proved to be in general very similar to model point Florida and was therefore not included in the discussion.

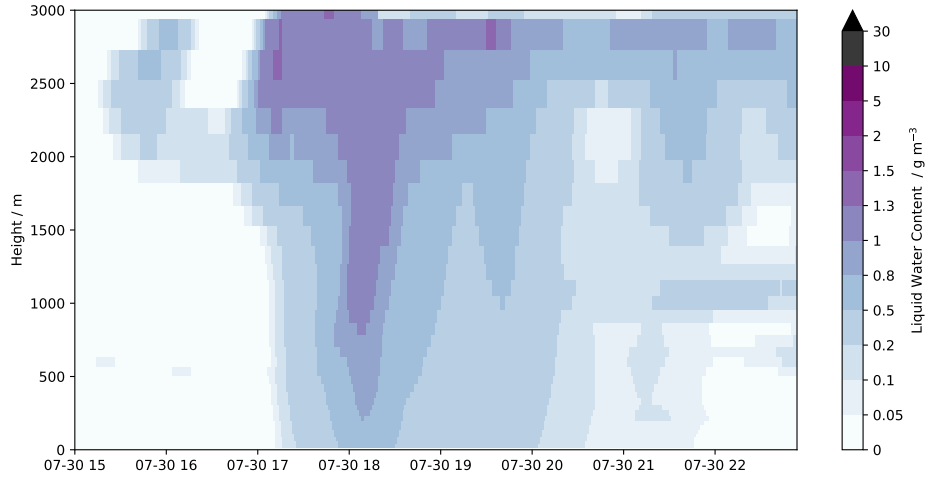

Figure 30: The distribution of predicted LWC in the atmosphere. LWC (g m^{-3}) is shown for model point Laksevåg for the time 15:00-23:00, for the lower 3 km of the atmosphere.

The vertical distribution of the terminal fall velocity of Laksevåg (Figure 31) also proved to be almost identical to Florida (Figure 21). The main difference is Laksevåg only have one enhanched core at 18:00, and it is missing the small enhancement in velocity in the lower level at 21:00.

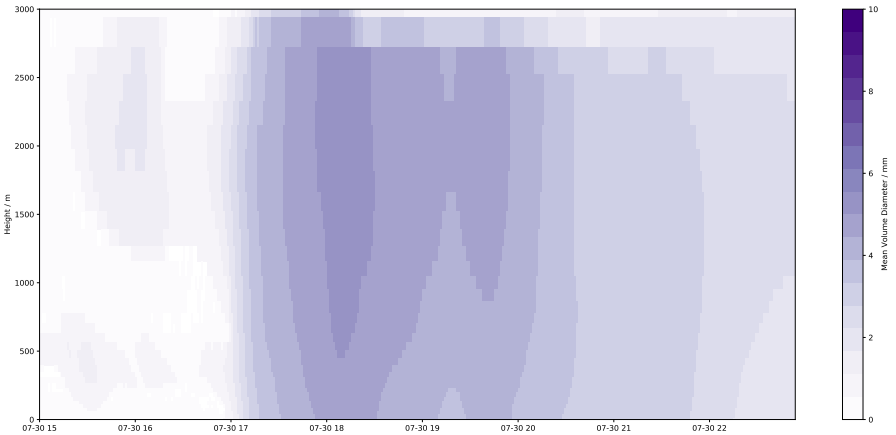

Figure 31: Vertical distribution of the predicted terminal fall velocity for the lower 3 km of the atmosphere (m s^{-1}). Showing the evolution for the precipitation event in model point Laksevåg, from 15:00-23:00 UTC.

References

R. Azad and A. Sorteberg. Extreme daily precipitation in coastal western Norway and the link to atmospheric rivers. *J. Geophys. Res. Atmos*, 122:2080–2095, 2017. doi: 10.1002/2016JD025615.

A. Battaglia, Elke Rustemeier, Ali Tokay, U. Blahak, and Clemens Simmer. Parsivel snow observations: a critical assessment. *Journal of Atmospheric and Oceanic Technology*, 27:333–344, 02 2010. doi: 10.1175/2009JTECHA1332.1.

L. Bengtsson, U. Andrae, T. Aspelien, Y. Batrak, J. Calvo, W. de Rooy, E. Gleeson, B. Hansen-Sass, M. Homleid, M. Hortal, KI. Ivarsson, G. Lenderink, S. Niemelä, KP. Nielsen, J. Onvlee, L. Rontu, P. Samuelsson, DS. Muñoz, A. Subias, S. Tijm, V. Toll, X. Yang, and Koltzow. The HARMONIE–AROME Model Configuration in the ALADIN–HIRLAM NWP System. *American Meteorological Society*, pages 1919–1935, 2017. doi: https://doi.org/10.1175/MWR-D-16-0417.1.

R. Conrick and C.F Mass. An Evaluation of Simulated Precipitation Characteristics during OLYMPEX. *Journal of Hydrometeorology 20(6)*, pages 1147–1164, 2019. doi: https://doi.org/10.1175/JHM-D-18-0144.1.

B.J.K. Engdahl, G. Thompson, and L. Bengtsson. Improving the representation of supercooled liquid water in the harmonie-arome weather forecast model. *Tellus A: Dynamic Meteorology and Oceanography*, 72(1):1–18, 2020. doi: 10.1080/16000870.2019.1697603. URL `https://doi.org/10.1080/16000870.2019.1697603`.

G.B. Foote and P.S. Du Toit. Terminal Velocity of Raindrops Aloft. *Journal of Applied Meteorology and Climatology 8(2)*, pages 249–253, 1969. doi: https://doi.org/10.1175/1520-0450(1969)008\%3C0249:TVORA\%3E2.0.CO;2.

C. Huang, S. Chen, A. Zhang, and Y. Pang. Statistical Characteristics of Raindrop Size Distribution in Monsoon Season over South China Sea. *Remote Sens 13 2878*, pages 1985–2000, 2021. doi: https://doi.org/10.3390/rs13152878.

ITAS. ITAS GFI Manual 20160518. *UiB*, pages 1–3, 2005. URL `https://wiki.uib.no/gfi/images/9/9e/ITAS_GFI_Manual_20160518.pdf`.

M. Kähnert, H. Sodemann, W.C de Rooy, and T.M. Valkonen. On the Utility of Individual Tendency Output: Revealing Interactions between Parameterized Processes during a Marine Cold Air Outbreak. *Weather and forecasting 36(6)*, pages 1985–2000, 2021. doi: https://doi.org/10.1175/WAF-D-21-0014.1.

A. Läderach and H. Sodemann. A revised picture of the atmospheric moisture residence time. *Geophys. Res. Lett*, page 924–933, 2016. doi: doi:10.1002/2015GL067449.

J.S. Marshall and W.Mc.K. Palmer. The Distribution of Raindrops with Size. *J. Meteor*, pages 165–166, 1948. doi: https://doi.org/10.1175/1520-0469(1948)005\%3C0165:TDORWS\%3E2.0.CO;2.

Germany METEK. MRR Physical Basics. *Meteorologische Messtechnik GmbH*, pages 1–20, 2009. URL `https://mpimet.mpg.de/fileadmin/atmosphaere/barbados/Instrumentation/MRR-physical-basics_20090707.pdf`.

Meteorologisk Institutt. *Intense byger med store konsekvenser i Sogn og Fjordane 30. juli 2019, 42 pages*. 2019.

M. Müller, M. Homleid, K.I. Ivarsson, M.A.Ø. Køltzow, M. Lindskog, K.H. Midtbø, U. Andrae, T. Aspelien, L. Berggren, D. Bjørge, P. Dahlgren, J. Kristiansen, R. Randriamampianina, M. Ridal, and O. Vignes. AROME-MetCoOp: A Nordic Convective-Scale Operational Weather Prediction Model. *Weather and Forecasting 32(2)*, pages 609–627, 2017. doi: https://doi.org/10.1175/WAF-D-16-0099.1.

Méteo-France. The Meso-NH Atmospheric Simulation System: Scientific Documentation Part III: Physics. *Centre National de la Recherche Scientifique*, pages 1–153, 2009. Specific Documentation.

Météo-France. Diagnostics in Horizontal Domains (DDH)- Variables and budget equations, in horizontal mean ARPEGE, ALADIN and AROME models. *Météo-France*, pages 1–75, 2019.

R.M. Rasmussen, J. Hallett, R. Purcell, S.D. Landolt, and J. Cole. The Hotplate Precipitation Gauge. *Journal of Atmospheric and Oceanic Technology 28(2)*, pages 148–164, 2011. doi: https://doi.org/10.1175/2010JTECHA1375.1.

T. H. Raupach and A. Berne. Correction of raindrop size distributions measured by parsivel disdrometers, using a two-dimensional video disdrometer as a reference. *Atmospheric Measurement Techniques*, 8(1):343–365, 2015. doi: 10.5194/amt-8-343-2015. URL `https://amt.copernicus.org/articles/8/343/2015/`.

R.R. Rogers and M.K. Yau. *A Short Course in Cloud Physics*. Butterworth-Heineman: Elsevier, 3 edition, 1989.

Y. Seity, P. Brousseau, S. Malardel, G. Hello, P. Bénard, F. Bouttier, C. Lac, and V. Masson. The AROME-France Convective-Scale Operational Model. *Mon Wea Rev*, page 976– 991, 2011. doi: h10.1175/2010MWR3425.1.

Varsom SeNorge. Se snøkart og klimakart for hele norge. *accessed: 20.05.2022*. URL `https://www.senorge.no/map`.

J. Testud, S. Oury, R.A. Black, and D. Xiankang. The Concept of "Normalized" Distribution to Describe Raindrop Spectra: A Tool for Cloud Physics and Cloud Remote Sensing. *Journal of Applied Meteorology and Climatology 40(6)*, pages 1118–1140, 2000. doi: https://doi.org/10.1175/1520-0450(2001)040\%3C1118:TCONDT\%3E2.0.CO;2.

E.J. Thompson, S.A. Rutledge, B. Dolan, and M. Thurai. Drop Size Distributions and Radar Observations of Convective and Stratiform Rain over the Equatorial Indian and West Pacific Oceansa. *Journal of the Atmospheric Science 72(11)*, pages 4091–4125, 2015. doi: https://doi.org/10.1175/JAS-D-14-0206.1.

G. Thompson, R.M. Rasmussen, and K. Manning. Explicit Forecasts of Winter Precipitation Using an Improved Bulk Microphysics Scheme. Part I: Description and Sensitivity Analysis. *Monthly Weather Review 132(2)*, pages 519–542, 2004. doi: https://doi.org/10.1175/1520-0493(2004)132\%3C0519:EFOWPU\%3E2.0.CO;2.

G. Thompson, P.R. Field, R.M. Rasmussen, and W.D. Hall. Explicit Forecasts of Winter Precipitation Using an Improved Bulk Microphysics Scheme. Part II: Implementation

of a New Snow Parameterization. *Monthly Weather Review 136(12)*, pages 5095–5115, 2008. doi: https://doi.org/10.1175/2008MWR2387.1.

Teresa Valkonen, Patrick Stoll, Yurii Batrak, Morten Køltzow, Thea Maria Schneider, Emmy E. Stigter, Ola B. Aashamar, Eivind Støylen, and Marius O. Jonassen. Evaluation of a sub-kilometre nwp system in an arctic fjord-valley system in winter. *Tellus A: Dynamic Meteorology and Oceanography*, 72(1):1–21, 2020. doi: 10.1080/16000870.2020.1838181. URL https://doi.org/10.1080/16000870.2020.1838181.

L. Wen, K. Zhao, G. Zhang, M. Xue, B. Zhou, S. Liu, and X. Chen. Statistical characteristics of raindrop size distributions observed in East China during the Asian summer monsoon season using 2-D video disdrometer and Micro Rain Radar data. *JGR Atmospheres*, pages 165–166, 2016. doi: https://doi.org/10.1002/2015JD024160.

L. Wen, K. Zhao, G. Zhang, S. Liu, and G. Chen. Impacts of Instrument Limitations on Estimated Raindrop Size Distribution, Radar Parameters, and Model Microphysics during Mei-Yu Season in East China. *Journal of Atmospheric and Oceanic Techonology 34(5)*, pages 1021–1037, 2017. doi: https://doi.org/10.1175/JTECH-D-16-0225.1.

P.T. Willis. Functional Fits to Some Observed Drop Size Distributions and Parameterization of Rain. *Journal of the Atmospheric Science 41(9)*, pages 1648–1661, 1984. doi: https://doi.org/10.1175/1520-0469(1984)041\%3C1648:FFTSOD\%3E2.0.CO;2.

YES. Hotplate^{tm} TOTAL PRECIPITATION SENSOR MODEL TPS-3100. *Yankee Environmental Systems*, pages 1–3, 2005. URL https://psl.noaa.gov/data/obs/instruments/HotPlate.pdf.

Meteorologisk Institutt YR. Nedbørvarsel i kart og graf. *accessed: 29.05.2022*, 2022. URL https://hjelp.yr.no/hc/no/articles/209295525-NÃěvarsel-FÃÿlg-med-pÃě-nedbÃÿren-med-vÃěrt-sanntids-nedbÃÿrvarse

J.P. Zagrodnik, L.A. Mcmurdie, and R.A. Houze JR. Stratiform Precipitation Processes in Cyclones Passing over a Coastal Mountain Range. *Journal of the Atmospheric Sciences 75(3)*, pages 983–1004, 2018. doi: 10.1175/JAS-D-17-0168.1.